SMC5/6-Mediated Plasmid Silencing is Directed by SIMC1-SLF2 and Antagonized by the SV40 Large T Antigen

Martina Oravcová[1], Minghua Nie[1], Takanori Otomo[2,3], and Michael N. Boddy[1,3]

[1]Department of Molecular and Cellular Biology, The Scripps Research Institute, La Jolla, CA 92037, USA.

[2]San Diego Biomedical Research Institute, San Diego, CA 92121, USA.

[3]Co-corresponding Authors: nboddy@scripps.edu and totomo@sdbri.org

Running Head: SIMC1 antagonizes plasmid gene expression.

Keywords: SIMC1, C5orf25, Nse5, SLF2, NSMCE5, SMC5, SMC6.

Abstract

SMC5/6 is unique amongst the Structural Maintenance of Chromosomes (SMC) complexes in its ability to repress transcription from extrachromosomal circular DNA (ecDNA), including viral genomes and plasmids. Previously, we showed that human SMC5/6 is regulated by two mutually exclusive subcomplexes—SIMC1-SLF2 and SLF1/2—the counterparts of yeast Nse5/6 (Oravcová, eLife, 2022). Notably, only SIMC1-SLF2 recruits SMC5/6 to SV40 Large T antigen (LT) foci in PML nuclear bodies (PML NBs), suggesting that these regulatory subcomplexes direct distinct roles of SMC5/6 on chromosomal versus ecDNA. However, their roles in plasmid repression remain unclear. Here, we demonstrate that SMC5/6-mediated repression of plasmid transcription depends exclusively on SIMC1-SLF2, whereas SLF1/2 is dispensable. Reinforcing its specialized role in ecDNA suppression, SIMC1-SLF2 does not participate in SMC5/6 recruitment to chromosomal DNA lesions. We further show that plasmid silencing requires a conserved interaction between SIMC1-SLF2 and SMC6, mirroring the functional relationship observed between yeast Nse5/6 and Smc6. As for viral silencing, plasmid repression depends on the SUMO pathway; however, unlike viral silencing, it does not require PML NBs. Additionally, we find that LT interacts with SMC5/6 and increases plasmid transcription to levels observed in SIMC1-SLF2-deficient cells–echoing the antagonistic roles of HBx (HBV) and Vpr (HIV-1) in viral genome repression. These findings expand the paradigm of viral antagonism against SMC5/6-mediated silencing, positioning LT as a novel player in this evolutionary tug-of-war.

37 **Introduction**

38 The Structural Maintenance of Chromosomes (SMC) complexes, present in both
39 prokaryotes and eukaryotes, are core modulators of chromosome architecture and
40 organization, supporting the development and homeostasis of all living organisms (1,2).
41 The SMC1/3 (cohesin) and SMC2/4 (condensin) complexes ensure accurate genome
42 propagation by folding chromosomes into distinct structures. Meanwhile, SMC5/6 plays a
43 key role in maintaining genome stability and integrity, contributing to processes such as
44 homologous recombination (HR), alternative lengthening of telomeres (ALT), and
45 ribosomal DNA (rDNA) replication (3-7). Recently, SMC5/6 has also been recognized as
46 a viral restriction factor, highlighting its broader role in managing extrachromosomal DNAs
47 (ecDNAs, (8-10)).

48 Beyond viral restriction, the repression of transcription from simple plasmid DNA
49 has also been added to the activities of the human SMC5/6 “Swiss Army knife” of DNA
50 manipulation (8-12). SMC5/6 selectively represses the transcription of circular but not
51 linear plasmid DNA (12), which is likely related to their topological states. That is, DNA
52 that accumulates superhelical stress during transcription is the preferred binding
53 substrate for SMC5/6, whereas linear DNA that dissipates such tension is not stably
54 bound by the complex (12-15). Once DNA bound, SMC5/6 may further compact and
55 thereby restrict transcriptional activity on the ecDNA.

56 All SMC complexes share a fundamental structure consisting of a SMC
57 heterodimer connected by a kleisin protein. These complexes form a ring-like structure
58 that traps DNA. The SMC proteins have a bent-arm shape and can open to encircle DNA
59 when their ATPase head domains bind ATP, aiding DNA movement through the ring.

60 Kleisin plays a critical role for connecting and locking the SMC heads together (6,16-22).
61 The SMC5/6 complex is particularly adept at recognizing and compacting special DNA
62 structures, such as HR intermediates and supercoiled DNA (13,15,23,24).

63 The SMC5/6 complex is composed of a highly conserved "core" hexamer: the
64 SMC5/6 heterodimer and non-SMC-elements (NSE) 1-4 (9). A Kleisin (Nse4 in yeast;
65 NSMCE4 in human) and two interacting partners (Nse1 and Nse3 in yeast; NSMCE1 and
66 NSMCE3 in human) form a trimer that joins the SMC5/6 head domains. The SUMO ligase
67 Nse2 (NSMCE2 in human) attaches to the SMC5 arm. The complex's functional
68 specificity is further defined by non-core subunits, the Nse5/6 heterodimer (9,18,25).

69 Yeast Nse5/6 plays key roles in regulating Smc5/6's genome stability functions,
70 facilitating its chromatin loading, inhibiting its ATPase activity, and enhancing Nse2
71 SUMO ligase activity (19,26-32). Despite its critical regulatory roles, the identification of
72 a human Nse5/6-like complex lagged, largely due to the lack of cross-species protein
73 sequence conservation. Nevertheless, identified in proteomic approaches, the human
74 SLF1 (SMC5-SMC6 Complex Localization Factor 1)-SLF2 heterodimer (SLF1/2) was
75 shown to fulfill some genome stability roles performed by Nse5/6 in yeast (7). Interestingly,
76 however, with the possible exception of HIV-1 proviral DNA, the repression of viral DNA
77 transcription by SMC5/6 depends on SLF2 but not SLF1 (8,9,11). Therefore, SLF2 either
78 functions as a monomer in viral repression, or there is a cofactor that replaces SLF1 in
79 this role. Towards resolving this issue, we recently discovered SIMC1 as a missing link in
80 SMC5/6 regulation and demonstrated that the SIMC1-SLF2 complex is a human
81 counterpart of yeast Nse5/6 (33).

82 Our structural and mutational analyses revealed that SIMC1 and SLF2 contain
83 Nse5 and Nse6-like domains, respectively, which interact through a conserved interface.
84 SIMC1-SLF2 interacts with and directs SMC5/6 to subnuclear compartments at PML
85 nuclear bodies (PML NBs) induced by the SV40 polyomavirus large T antigen (LT).
86 Further, we showed that SIMC1-SLF2 and SLF1/2 are mutually exclusive subcomplexes
87 of SMC5/6 that likely support the distinct antiviral and DNA repair activities of the
88 holocomplex. Thus, SIMC1-SLF2 and SLF1/2 act as Nse5/6-like regulatory elements that
89 modulate the broad activities of the SMC5/6 complex (33).

90 Despite the foregoing advances, the specific roles of the SLF2-based SIMC1 and
91 SLF1 subcomplexes in SMC5/6 regulation remained unclear. Although we previously
92 proposed distinct functions for SIMC1-SLF2 and SLF1/2 in ecDNA silencing and DNA
93 repair, respectively, these mechanisms had yet to be demonstrated. Additionally,
94 SUMOylation, PML NBs, and SV40 LT were implicated in the regulation of SMC5/6-based
95 ecDNA silencing, but their actual contributions remained untested. Here, we address
96 these gaps directly. In line with our prior model, we show that SIMC1-SLF2, but not
97 SLF1/2, mediates plasmid silencing through a direct and evolutionarily conserved
98 interaction with SMC6. Conversely, SLF1/2 specifically recruits SMC5/6 to DNA lesions.
99 Furthermore, we demonstrate that plasmid silencing is facilitated by the SUMO pathway
100 but, unlike the SMC5/6-mediated silencing of HBV (34), does not require PML NBs. Lastly,
101 we reveal that SV40 LT binds SMC5/6 and antagonizes plasmid silencing, thereby adding
102 polyomaviruses to the growing list of pathogenic viruses that counteract SMC5/6-based
103 transcriptional repression.
104

105 **Results**

106 **SIMC1-SLF2 associates with SMC6 through a conserved patch**

107 Our previous structural analysis revealed that the Nse5-like domain of SIMC1 ($SIMC1^{Nse5}$)
108 and the Nse6-like domain of SLF2 ($SLF2^{Nse6}$) both adopt α-solenoid-like structures (33).
109 These domains interact in a head-to-tail orientation, forming an ellipsoid-shaped dimer
110 (**Figure 1A**). This dimerization clusters conserved residues from the N-terminus of
111 $SIMC1^{Nse5}$ and the C-terminus of $SLF2^{Nse6}$ at one edge of the ellipsoid (**Figure 1B**). We
112 previously used a SIMC1 mutant harboring four substitutions in α1 of SIMC1 ($SIMC1^{combo}$,
113 **Figure 1B**) to demonstrate that this conserved patch of SIMC1 is essential for binding to
114 SMC6 and for the localization of the SMC5/6 complex at LT-containing PML NBs (33).

115 In this study, we extended our analysis to SLF2 by introducing two sets of
116 mutations into the Nse6-like region of SLF2 ($SLF2^{CTD}$; residues 635-1173): **mut 1**
117 (E1121A/K1122A/K1125D/C1126R/E1130K in α16) and **mut 2**
118 (T1138R/K1141E/D1142R/A1145R/G1149E in the subsequent loop and α17). These
119 mutations were designed to disrupt charge interactions, hydrogen bonds, and van der
120 Waals contacts, following the same strategy used with $SIMC1^{combo}$ to disrupt binding (33).
121 Using HEK293 cells co-expressing FLAG-tagged $SLF2^{CTD}$ mutants, GFP-tagged SIMC1
122 and Myc-tagged SMC6, we performed GFP pull-downs followed by Western blot analysis
123 (**Figure 1C**). Wild-type $SLF2^{CTD}$ interacted with both SIMC1 and SMC6 (Lane 1), whereas
124 both **mut 1** and **mut 2** disrupted SMC6 binding while preserving the interaction with
125 SIMC1 (Lanes 2, 3).

126 We also examined several control mutants. To confirm the SIMC1-SMC6 interface,
127 we introduced a new SIMC1 control mutant containing four

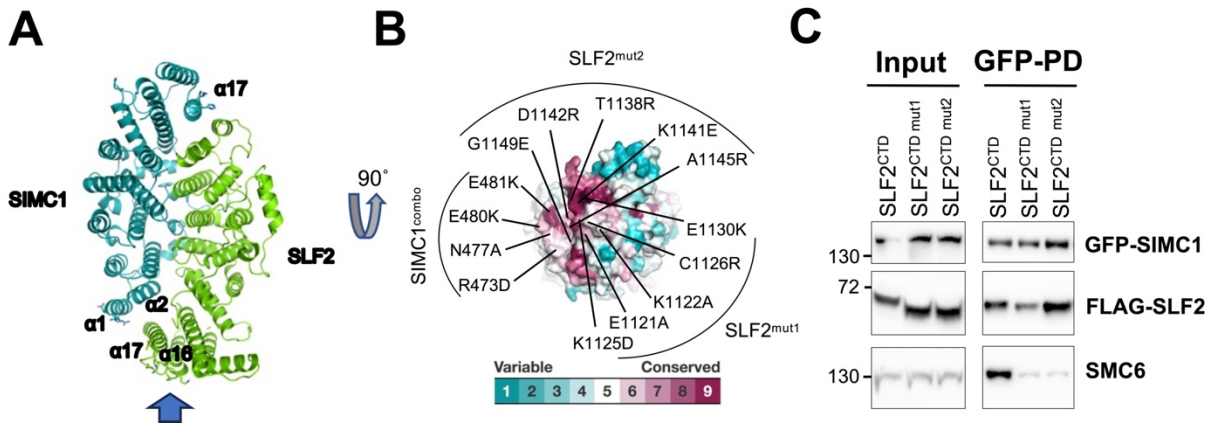

Figure 1: SIMC1-SLF2 composite surface patch is required for SMC6 association. **(A)** The cryo-EM structure of the SIMC1-SLF2 complex (PDB ID: 7T5P) (33). Residues mutated for interaction analysis are shown with side chains. The arrow at the bottom indicates the viewing angle for (B). **(B)** Conservation mapping on the surface of SIMC1-SLF2 complex, showing the N-terminus of SIMC1 and the C-terminus of SLF2. Conservation scores obtained from the Consurf server (35) are shown by the color graduation as indicated. Amino acids mutated in SIMC1^{combo} (R473D/N477A/E480K/E481K in α1 of SIMC1), SLF2 mut1 (E1121A/K1122A/K1125D/C1126R/E1130K in α16 of SLF2) and SLF2 mut2 (T1138R/K1141E/D1142R/A1145R/G1149E in α17 of SLF2) are labeled. **(C)** Western blot of GFP-Trap immunoprecipitation from HEK293 cells transfected with plasmids expressing GFP-SIMC1, Myc-SMC6, and FLAG-tagged C-terminal domain (CTD) of SLF2, either WT or containing mutations (mut1, mut2). Input and GFP PD were detected with anti-GFP, FLAG, or SMC6 antibody.

146 substitutions (Q842A/H846A/K849E/D857R) in α17, located at the opposite end of the
147 ellipsoid, away from the predicted SMC6 contact surface (**Figure 1A**). This SIMC1 mutant
148 bound to SLF2 but more weakly than wild-type SIMC1 (**Figure 1—figure supplement**
149 **1A**). This was an unexpected finding that is difficult to rationalize based on the structure.
150 However, despite the reduced SLF2 association, it fully retained its interaction with SMC6,
151 indicating that the residues mutated in SIMC1^{combo} are specific to the SMC6 interface. In
152 this experiment using overexpressed proteins, SIMC1 and SMC6 appear capable of
153 maintaining their association during the pull-down even without stoichiometric SLF2. We
154 then evaluated the most C-terminal residues of SLF2 (1161–1173), which are
155 unstructured. Despite their conservation, deleting these residues (SLF2$^{635-1160}$) did not
156 affect SMC6 binding (**Figure 1—figure supplement 1B**). Collectively, these results
157 confirm that the conserved surface patch of SIMC1-SLF2 is essential for SMC6 binding.
158

159 **SIMC1-SLF2 subcomplex contacts the neck region of SMC6**

160 We used AlphaFold-Multimer (36) to predict the structure of the SIMC1-SLF2-SMC6
161 complex (**Figure 2A, Figure 2—figure supplement 1A**). The resulting high-confidence
162 model, as assessed by the predicted aligned error (PAE) plot (**Figure 2—figure**
163 **supplement 1B**), aligns well with mutational data and highlights the conserved surface
164 patch of SIMC1-SLF2 as the interface with SMC6 (**Figure 2A**). SMC6 is a long, hairpin-
165 like polypeptide in which its N- and C-termini fold together to form the ATPase “head”
166 domain at one end. The “hinge” domain at the bending end mediates heterodimerization
167 with SMC5 (**Figure 2—figure supplement 1A**). Connecting the head and hinge is a

168 flexible coiled-coil; the portion adjacent to the head is referred to as the “neck” (**Figure**
169 **2A**).

170 In the model, the conserved SIMC1-SLF2 surface patch interacts with C-terminal
171 residues of SMC6, centered on the neck and opposite the ATPase active site where it
172 dimerizes with SMC5’s ATPase domain (21,30). This interface shows excellent shape

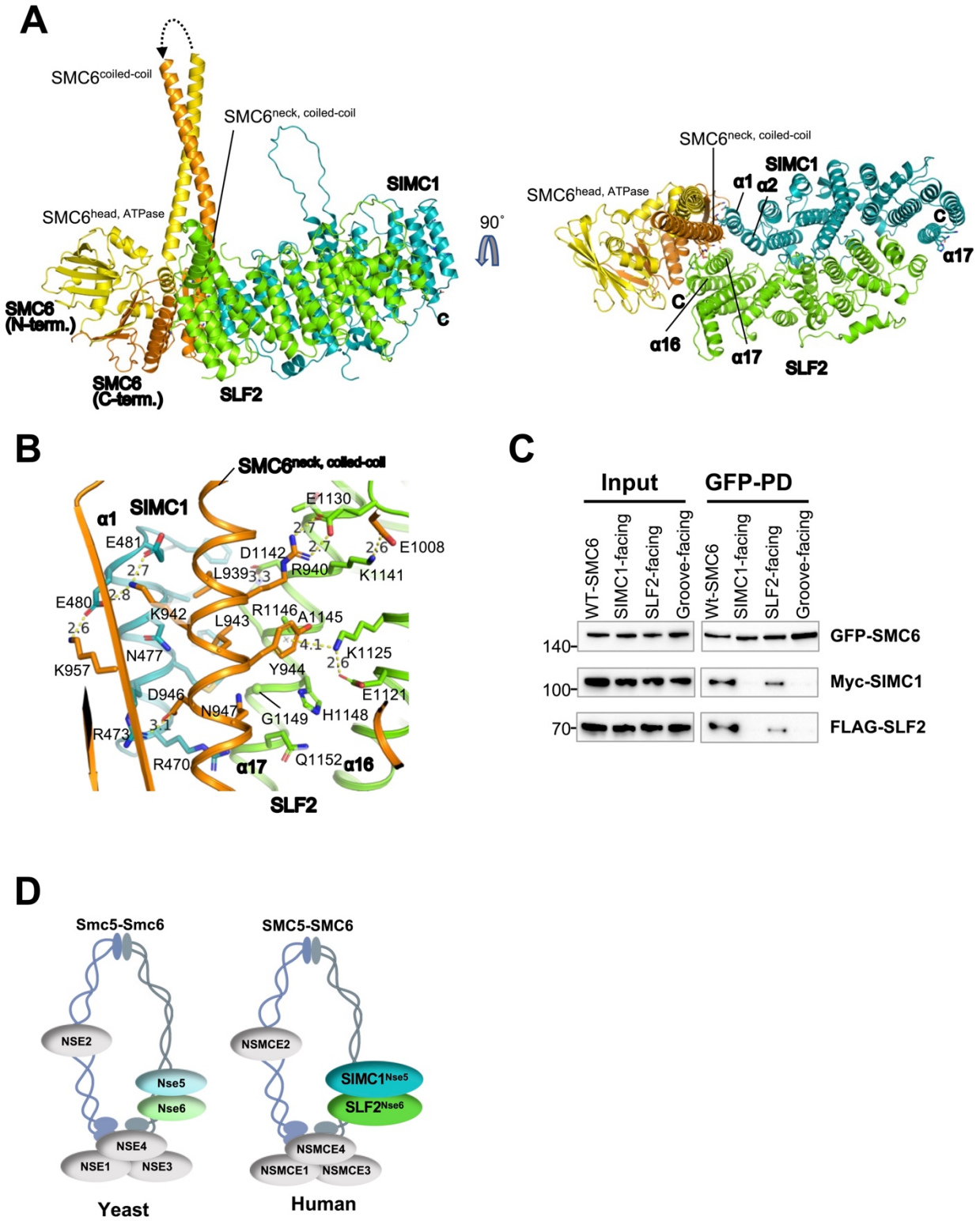

Figure 2: SIMC1-SLF2 subcomplex contacts the neck region of SMC6.
(A) The AlphaFold-Multimer model of the SIMC1^{Nse5}-SLF2^{Nse6}-SMC6 complex. The disordered regions in the N- and C-termini, the hinge domain, and the majority of the coilded-coil that do not contact SIMC1-SLF2 are omitted for clarity. The entire model and

178 the Predicted Aligned Error (PAE) plot of the prediction are shown in **Figure 2 - figure**
179 **supplement 1**. Residues mutated for interaction analysis are shown with side chains. **(B)**
180 A close-up view of the interface between SMC6's neck and the composite patch of
181 SIMC1-SLF2. **(C)** Western blot of GFP-Trap immunoprecipitation from HEK293 cells
182 transfected with plasmids expressing 2Myc-SIMC1, FLAG-SLF2^{CTD}, and WT or mutant
183 GFP-SMC6 (SIMC1-facing: K942A, D946A, K957A; SLF2-facing: R940A, Y944A, N947A;
184 groove-facing: L939A, R940A, K942A, L943A). Input and GFP PD were detected with
185 anti-GFP, FLAG, or Myc antibody. **(D)** Schematic of yeast (left) and human (right) SMC5/6
186 complex illustrating positions of its subunits within the complex and Nse5/Nse6 and
187 SIMC1/SLF2 cofactors, respectively, interacting with the neck region of SMC6.

188 complementarity—SMC6's convex neck helix fits snugly into the concave surface formed
189 by α1 and α2 of SIMC1 and α17 of SLF2 (**Figure 2A**). Additional interactions arise from
190 SLF2's α16 and the α16-α17 loop with SMC6's head residues, spanning a total buried
191 surface area of 1516 Å².

192 This model explains the roles of the amino acids altered in our binding studies
193 (**Figure 2B; Figure 2—figure supplement 1C, D**). The four residues modified in
194 SIMC1^{combo} all make direct contact with SMC6's neck helix, including three salt bridges:
195 R473^{SIMC1}-D946^{SMC6}, E480^{SIMC1}-K957^{SMC6}/K942^{SMC6}, and E481^{SIMC1}-K942^{SMC6}. The SLF2
196 mutations also engage SMC6's neck region, forming salt bridges (E1130^{SLF2}-R940^{SMC6}
197 and K1141^{SLF2}-E1008^{SMC6}), a cation-π interaction (K1125^{SLF2}-Y944^{SMC6}), and multiple
198 van der Waals contacts (**Figure 2A; Figure 2—figure supplement 1C, D**). Thus, the
199 model and mutational data are consistent.

200 Next, we validated these SMC6's interface contacts using alanine substitutions.
201 We introduced three sets of mutations: 1) **SIMC1-facing** residues (K942A/D946A/K957A),
202 which form salt bridges with SIMC1; 2) **SLF2-facing** residues (R940A/Y944A/N947A),
203 which form salt bridges and polar and hydrophobic contacts with SLF2; 3) **SIMC1-SLF2-**
204 **groove-facing** (L939A/R940A/K942A/L943A), which alters two leucines that insert into a
205 hydrophobic groove between α1 of SIMC1 and α17 of SLF2, together with the SIMC1-
206 and SLF2-facing residues (K942 and R940, respectively) (**Figure 2B**). When these SMC6
207 mutants were co-expressed with SIMC1 and SLF2, pull-down assays showed significantly
208 reduced or abolished binding (**Figure 2C, lane 2-4**). Thus, our mutational data strongly
209 support the AlphaFold model.

210 We conclude that SIMC1-SLF2 associates with the neck region of SMC6, opposite
211 the ATPase active site used for heterodimerization with SMC5 (**Figure 2D; Figure 2—**
212 **figure supplement 1A**). A recent cryo-EM study on the *S. cerevisiae* Smc5/6 complex
213 similarly demonstrated that Nse5/6 engages with the neck region of Smc6 (30),
214 reinforcing the idea that this mode of interaction is evolutionarily conserved (**Figure 2D**).
215 This has implications for the function of SIMC1-SLF2 in the regulation of SMC5/6 activity,
216 based on the findings for yeast Nse5/6 (see discussion).
217

218 **SMC5/6 mediated plasmid silencing requires the Nse5/6-like SIMC1-SLF2 complex**

219 To examine the role of SIMC1 and SLF2 in SMC5/6-mediated episomal DNA silencing,
220 we used CRISPR-Cas9 to create U2OS SIMC1$^{-/-}$ or SLF2$^{-/-}$ cells. We first compared the
221 expression of a transfected GFP reporter plasmid between wild-type (WT) and null cells.
222 GFP transcripts, as quantified by RT-qPCR, showed a strong increase over WT in both
223 SIMC1$^{-/-}$ and SLF2$^{-/-}$ cells (**Figure 3A**). This increase in GFP transcripts was not due to
224 an increase in average plasmid copy number in SLF2 null cells, versus WT, as determined
225 by qPCR (**Figure 3–figure supplement 1A**). We then used fluorescence activated cell
226 sorting (FACS) to monitor GFP expression (37) and found that both SIMC1$^{-/-}$ and SLF2$^{-/-}$
227 cells expressed significantly more GFP than WT (**Figure 3B**)**.** Importantly, expressing WT
228 SIMC1 or SLF2 in the corresponding null cells reduced reporter expression to levels
229 observed in WT cells (**Figure 3B**), demonstrating the involvement of SIMC1-SLF2 in
230 plasmid silencing. Notably, however, SLF2^{mut1} that abolishes the SIMC1-SLF2 interaction
231 with SMC6 (**Figure 1C**) did not reduce reporter expression in SLF2$^{-/-}$ cells, despite being
232 well expressed (**Figure 3B–figure supplement 1B**). Importantly, in keeping with related

233 studies (38-40), we found that the effect of SLF2 on GFP expression was lost upon
234 integration of the GFP reporter plasmid into the genome (**Figure 3–figure supplement**
235 **1C**). Together, these findings demonstrate that SIMC1-SLF2, and their interaction with
236 SMC6, are required for the selective repression of episomal plasmid DNA.
237
238
239

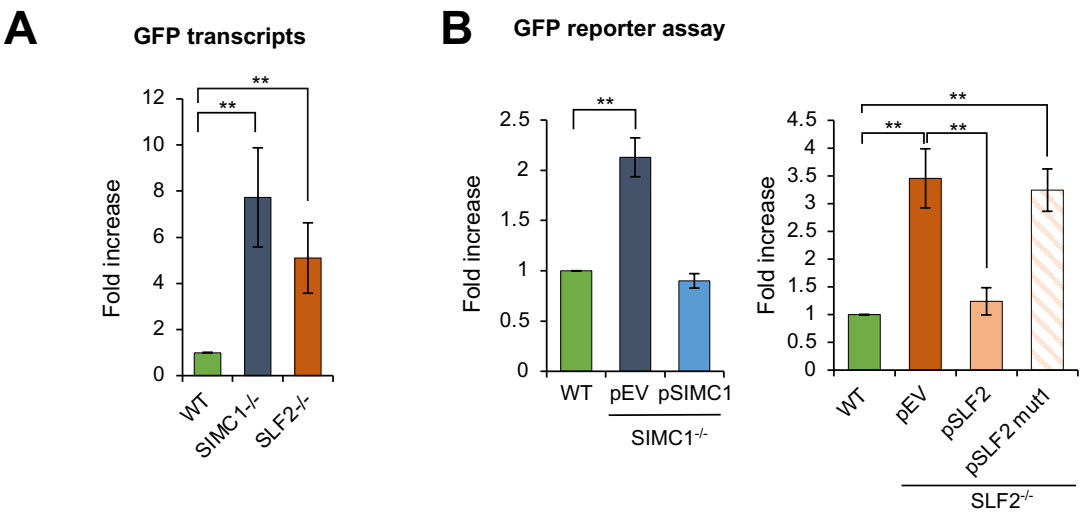

Figure 3: SIMC1/SLF2-SMC6 interaction is critical for plasmid silencing.
(A) Expression of a GFP reporter transiently transfected into U2OS WT and SIMC1$^{-/-}$ or SLF2$^{-/-}$ cell lines was measured by reverse transcription-quantitative PCR 72 hours after transfection. GFP expression was normalized to the expression of beta-actin (mean ± s.d. from n=4 independent experiments, two-tailed unpaired t-test; (**) $p<0.005$). **(B)** U2OS WT, SIMC1$^{-/-}$ or SLF2$^{-/-}$ cells with integrated empty vector or vector expressing SIMC1 or SLF2 variants (WT, mut1), respectively, were transiently transfected with GFP reporter. After 72 hours, GFP intensity was measured by FACS and is displayed relative to GFP intensity measured in WT cells. Data are the average ± s.d. from n=3 independent experiments, two-tailed unpaired t-test; (**) $p<0.005$). No significant difference ($p>0.05$) was found between WT and SIMC1$^{-/-}$ + pSIMC1 (left panel), or between WT and SLF2$^{-/-}$ + pSLF2 (right panel).

254 **SIMC1 and SLF1 direct SMC5/6 to plasmid silencing and DNA repair, respectively**

255 We previously showed that SLF1/2 and SIMC1-SLF2 form mutually exclusive complexes
256 with SMC5/6 and recruit it to distinct cellular locations (33). Specifically, epitope-tagged
257 SLF1 colocalized with gamma-H2AX at laser stripes, whereas SIMC1 did not. Here we
258 more directly examined the roles of SLF1 and SIMC1 in recruiting SMC5/6 to DNA
259 damage sites. To this end, we induced localized DNA lesions using laser microirradiation
260 in WT, SLF1$^{-/-}$, and SIMC1$^{-/-}$ U2OS cells. In WT and SIMC1$^{-/-}$ cells SMC5/6 accumulated
261 at laser-induced lesions marked by gamma-H2AX, whereas no such accumulation was
262 seen in SLF1$^{-/-}$ cells (**Figure 4A**). Thus, SLF1 but not SIMC1 plays a critical role in
263 directing SMC5/6 to DNA damage sites. Conversely, when comparing GFP reporter
264 expression in WT and SLF1 null cells, we found no change in GFP levels in the absence
265 of SLF1 (**Figure 4B**). Thus, unlike SIMC1, SLF1 does not play a role in SMC5/6-mediated
266 plasmid silencing, which is consistent with what has been observed in SLF1$^{-/-}$ HepG2
267 cells (10).

268

269

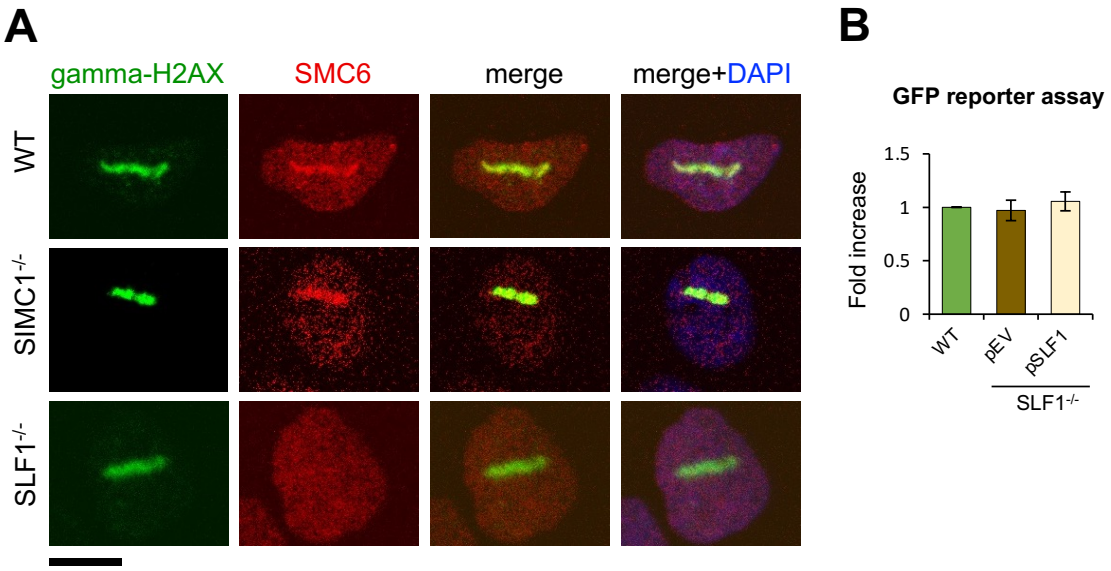

Figure 4: SLF1 is involved in SMC5/6 DNA damage repair, not plasmid silencing. **(A)** Representative immunofluorescence images of U2OS WT, SIMC1$^{-/-}$, SLF1$^{-/-}$ cells exposed to laser microirradiation upon treatment with 50 uM angelicin and 1 ug/ml Hoechst 33342 for 30 min. One hour after microirradiation, cells were pre-extracted, fixed and stained with gamma-H2A.X (phosphorylation of histone H2A.X Ser139; green), SMC6 (red) antibodies and DAPI (blue). Scale bar 10 µm. **(B)** GFP intensity was measured by flow cytometry 72 hr after reporter transient transfection in U2OS WT cells or SLF1$^{-/-}$ cells with integrated empty vector or stably expressing SLF1. Data are the average ± s.d. from n=3 independent experiments, two-tailed unpaired t-test (p-value >0.05).

282 **SUMOylation supports plasmid repression**

283 Given that SIMC1 contains SUMO interacting motifs (SIMs), and the SMC5/6 complex is
284 a SUMO ligase that contains other SUMO-interacting interfaces, we also tested for a
285 potential involvement of the SUMO pathway in plasmid silencing (33,41,42). Cells were
286 treated with the SUMO pathway inhibitor (SUMOi), TAK-981 (43). We observed a strong
287 dose-dependent increase in reporter gene expression in both U2OS and RPE cells
288 (**Figure 5—figure supplement 1A, B**), supporting an involvement of the SUMO pathway
289 in plasmid silencing. This is consistent with the broadly observed transcriptionally
290 repressive activity of SUMOylation (44,45). Interestingly, SUMOi treatment does not
291 significantly increase the level of GFP reporter expression in SIMC1$^{-/-}$ and SLF2$^{-/-}$ over its
292 effect on WT, despite the pre-existing defect in plasmid silencing in SIMC1 and SLF2 null
293 cell lines (**Figure 5A**). The lack of additivity between SUMOi and SIMC1$^{-/-}$ or SLF2$^{-/-}$
294 suggests that SMC5/6-mediated plasmid silencing operates in large part under the broad
295 "umbrella" of SUMOylation-based transcriptional repression. Intriguingly, when the GFP
296 reporter plasmid was integrated into the genome, its expression was unaffected by
297 SUMOi treatment in either WT or SLF2^{-}/$^{-}$ U2OS cells (Figure 5—figure supplement 1C).
298 This was somewhat unexpected given the broadly inhibitory effect of SUMO on
299 transcription. One possibility is that the dynamic range of transcriptional regulation is
300 larger for episomal DNA, resulting in the muted response of the integrated reporter. This
301 phenomenon merits further investigation.

302

303

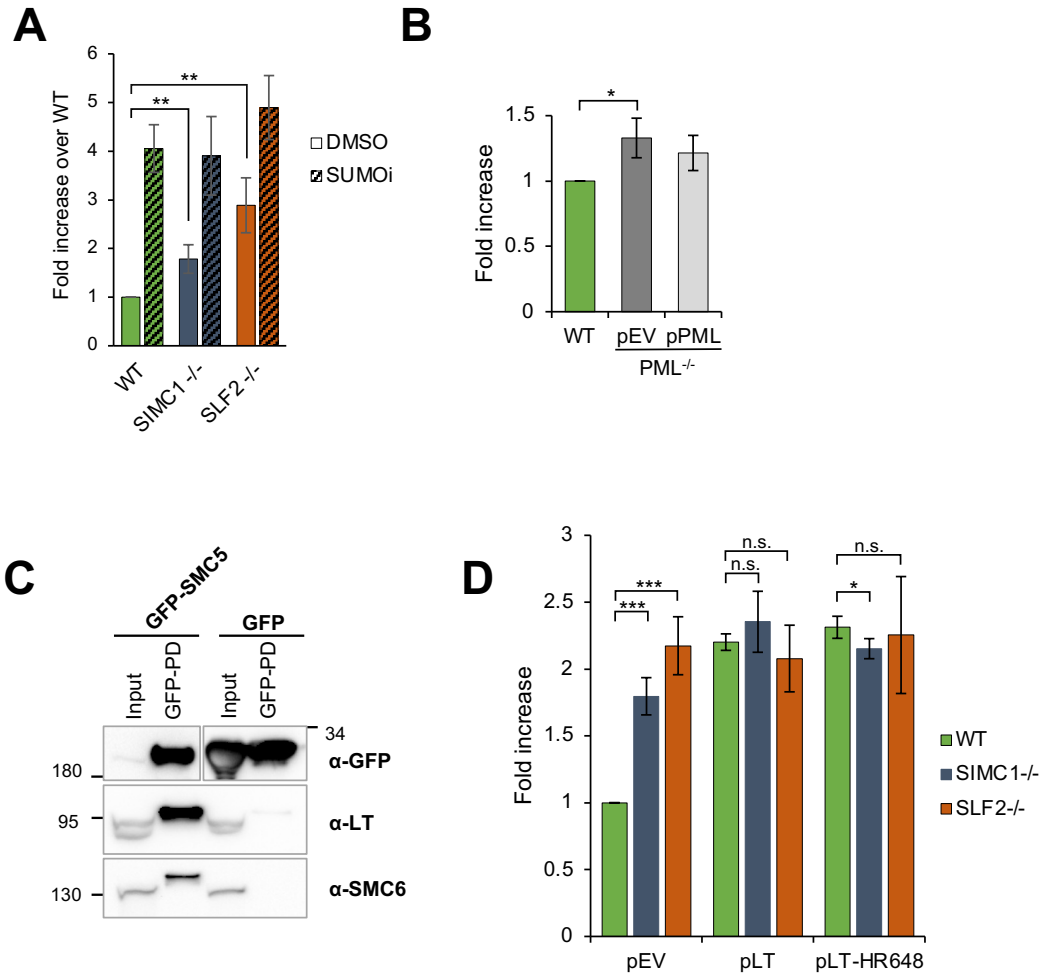

Figure 5: Plasmid silencing depends on the SUMO pathway and LT, not PML NBs. **(A)** U2OS WT, SIMC1$^{-/-}$ or SLF2$^{-/-}$ cells were transiently transfected with GFP reporter and treated with 100 nM TAK-981(SUMOi) or DMSO at the same time. After 72 hours, GFP intensity was determined by FACS. Data are normalized to WT cells treated with DMSO and represent the average ± s.d. from n=4 independent experiments, two-tailed unpaired t-test; (**) $p<0.005$. No significant difference was found between WT and SIMC1$^{-/-}$ or SLF2$^{-/-}$ when treated with SUMOi ($p>0.05$). **(B)** U2OS WT or PML$^{-/-}$ cells with integrated empty vector or vector expressing PML, respectively, were transiently transfected with GFP reporter. Intensity of GFP was measured by FACS 72 hours after transfection. Data are the average ± s.d. from n=3 independent experiments, two-tailed unpaired t-test; (*) $p<0.05$). No significant difference ($p>0.05$) was found between WT and PML$^{-/-}$ + pPML. **(C)** Western blot of GFP-trap immunoprecipitation from HEK293 cells transiently transfected with either GFP-SMC5 or GFP alone in combination with SV40 vector expressing LT and Myc-SMC6. Signals were visualized using GFP, LT and SMC6 antibodies. **(D)** GFP intensity measured by FACS in U2OS WT, SIMC1$^{-/-}$ or SLF2$^{-/-}$ cells with integrated empty vector, vector expressing large T antigen (LT) or LT-HR684 variant, respectively that were transiently transfected with GFP reporter for 72 hours. Data are the average ± s.d. from n=4 independent experiments. (∗) $p<0.05$; (∗∗∗) $p<0.0005$; (n.s.) $p>0.05$ (two-tailed unpaired t-test).

324 **PML NBs are not required for plasmid silencing**

325 We previously showed that SIMC1-SLF2 directs SMC5/6 to LT antigen-containing SV40
326 replication centers at PML NBs (33). Moreover, SMC5/6-mediated restriction of HBV
327 occurs at PML NBs (34,46) and, the localization of SMC5/6 at PML NBs is SLF2-
328 dependent in HepG2 and PHH cells (10,46). We also now find that SLF2 is required for
329 the localization of SMC5/6 to PML NBs in U2OS cells (**Figure 5—figure supplement 2**).
330 Based on the foregoing, PML NBs have been proposed, but not directly shown, to support
331 simple plasmid repression (10). Therefore, we tested the impact of PML NBs on plasmid
332 silencing by measuring GFP reporter expression in WT and PML$^{-/-}$ U2OS cells (47).
333 Compared to SIMC1 and SLF2 null cells, we observed only a minor increase in GFP
334 expression in PML$^{-/-}$ versus WT cells (**Figure 5B**). Moreover, the stable re-expression of
335 PML in PML$^{-/-}$ cells did not significantly reduce the level of GFP expression, as compared
336 to vector control, suggesting the slight increase observed is due to clonal variation from
337 CRISPR editing (**Figure 5B**). Thus, we conclude that PML NBs are not needed for the
338 SMC5/6-mediated silencing of plasmids.

339

340 **SV40 Large T antigen (LT) overcomes plasmid silencing**

341 Considering that HBx and Vpr antagonize SMC5/6 to induce HBV and HIV-1 transcription,
342 respectively (38,39,48), we tested if SV40 LT similarly impacts plasmid silencing. In this
343 regard, we previously found that SMC5/6 colocalizes with LT-induced nuclear foci at PML
344 NBs in a SIMC1-SLF2-dependent manner (33). Here, we show that ectopically expressed
345 LT coimmunoprecipitates with GFP-SMC5/6 but not a GFP control (**Figure 5C**). Therefore,
346 LT, like HBx and Vpr, may contact SMC5/6 to antagonize its ecDNA repression activity.

347 Indeed, the stable expression of LT in WT cells promoted GFP reporter plasmid
348 expression, as compared to WT cells with an empty vector control (**Figure 5D; Figure 5–**
349 **figure supplement 3A**). The host range defective mutant LT-HR684 had a similar effect
350 as WT LT, indicating that the C-terminus of LT, which inhibits the SV40 host range
351 restriction factor FAM111A (49), is not involved in overcoming plasmid repression (**Figure**
352 **5D**). Notably, the enhancement of plasmid DNA transcription by LT is not additive with
353 that already present in SIMC1$^{-/-}$ and SLF2$^{-/-}$ cells (**Figure 5D**). The epistatic relationship
354 between the positive effects of SIMC1$^{-/-}$, SLF2$^{-/-}$, and LT expression on plasmid
355 transcription indicates that LT overcomes SMC5/6-mediated repression. Interestingly, as
356 we observed with SUMOi, when the GFP reporter plasmid was integrated in WT or SLF2$^{-/-}$
357 U2OS cells, there was not a pronounced effect of LT on GFP expression (**Figure 5–figure**
358 **supplement 3B**). This is like the selective effect of HBx, whereby it overcomes the innate
359 repression of transcription from episomal but not chromosomal reporters (40).
360

361 **Discussion**

362 Our structural analyses indicate that SIMC1-SLF2 engages the SMC5/6 core at the neck
363 region of SMC6, situated opposite the ATPase active site. These findings, together with
364 recent cryo-EM analyses of the *S. cerevisiae* Smc5/6 complex (20,21,31), highlight a
365 conserved mode of interaction in which Nse5/6 or Nse5/6-like subunits bind to the
366 backside of SMC6's head domain. This binding site is ideal for allosteric regulation of the
367 ATPase and DNA-binding functions of the SMC5/6 family. Indeed, yeast Nse5/6 reduces
368 Smc5/6 ATPase activity and disrupts the Nse4 (kleisin)-Smc6 interface, which may open
369 the gate to enable topological DNA binding by Smc5/6 (**Figure 6**, (20,30,31)). The clear

370 overlap between our validated SIMC1-SLF2-SMC6 structure and that of yeast Nse5/6-
371 Smc6 suggests that SIMC1-SLF2, and its orthologue SLF1/2, may similarly modulate
372 SMC5/6 ATPase and DNA binding activities, albeit at distinct DNA targets.
373

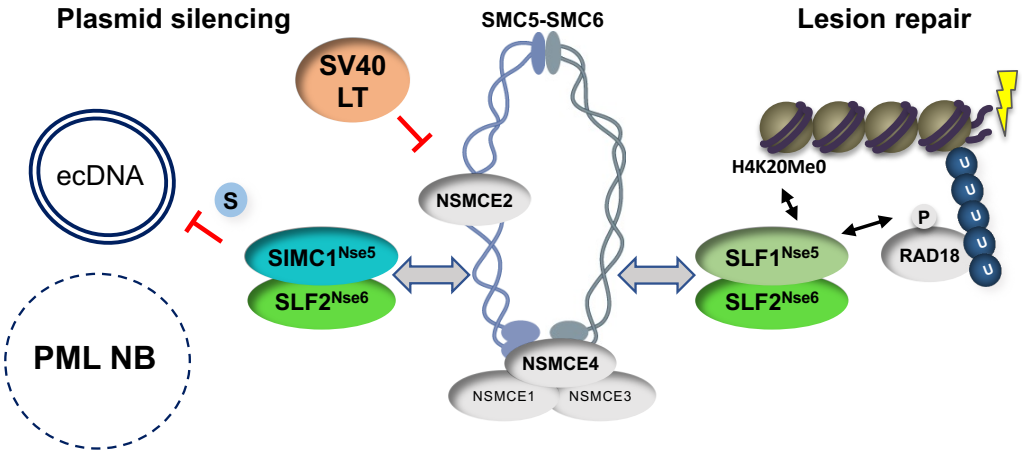

374
375 **Figure 6: SIMC1-SLF2 and SLF1/2 subcomplexes direct SMC5/6 to separate**
376 **pathways of plasmid silencing and DNA lesion repair.** SIMC1-SLF2 and SMC5/6-
377 mediated plasmid silencing is facilitated by the SUMO pathway and antagonized by SV40
378 LT. PML NBs are not involved in plasmid silencing. S stands for SUMO; U for ubiquitin.
379 Both SIMC1-SLF2 and SLF1/2 likely contact SMC6 directly through their conserved
380 Nse5/6-like domains, but the SIMC1 SIMs and SLF1 BRCT/ARD domains contact distinct
381 posttranslational modifiers to direct the complex to its separate roles.

382 The distinct targeting functions of the SIMC1 and SLF1-based SLF2 complexes is
383 underscored by our current analysis of microirradiated cells that lack each complex
384 (**Figure 4**). While the deletion of SLF1 abrogates SMC5/6 localization at DNA lesions, the
385 loss of SIMC1 has no effect (**Figure 4A**). On the other hand, SIMC1 is required for the
386 recruitment of SMC5/6 to LT-containing PML NBs (33). Lastly, we found that SLF1 does
387 not impact plasmid silencing (**Figure 4B**), consistent with several analyses of HIV-1, rAAV,
388 and HBV silencing (10,39,46,50) but contrasting with another study (51). It remains
389 unclear why this latter discrepancy exists. While there may still be overlapping functions
390 of SIMC1 and SLF1 to uncover at the organismal level, it is clear they support distinct
391 cellular responses to ecDNAs and DNA lesions (**Figure 6**).

392 In keeping with the SUMO-binding ability of SIMC1 (**Figure 6**, (42)), we found that
393 the inhibition of SUMOylation by TAK-981 strongly enhanced plasmid transcription
394 (**Figure 5–figure supplement 2**). This is likely a broad effect that includes the loss of
395 repressive modifications of transcription factors (45); as well as the lifting of SMC5/6-
396 mediated repression to enhance ecDNA transcription. A similar effect of TAK-981 was
397 seen on HIV-1 proviral DNA gene expression, which was elevated by SUMO inhibition to
398 a similar degree as that observed in SMC5Δ cells (51). The authors concluded that the
399 effect of TAK-981 was entirely through the inhibition of SMC5/6-mediated SUMOylation
400 (NSE2 subunit). This is different to our results, which show that SUMOylation inhibition
401 has a larger effect than the loss of the SIMC1-SLF2 complex on plasmid gene expression.
402 The distinct natures of the ecDNAs under study, plasmid versus HIV-1 proviral DNA, and
403 the genetic backgrounds may contribute to this difference. Nevertheless, our data support
404 a key role of the SUMO pathway in plasmid repression, and that SMC5/6 works within it.

405 Despite the fact that SIMC1-SLF2 localizes SMC5/6 to PML NBs that contain SV40
406 LT (31), and HBV is restricted at PML NBs (34), they are dispensable for plasmid silencing.
407 While the reason for the different impact of PML NBs in HBV versus simple plasmid
408 silencing remain unknown, it may be related to the natural localization of each ecDNA.
409 That is, HBV localizes to PML NBs as part of the viral life cycle, in a manner dependent
410 on the SUMOylation of its core protein (52). In contrast, the direct visualization of plasmids
411 revealed they are pan-nuclear and apparently excluded from PML NBs (53). It is also
412 noteworthy that a recent genome-scale CRISPR screen for repressors of rAAV
413 transcription identified all components of the SMC5/6 complex, including SIMC1 and
414 SLF2, but not SLF1 or PML (50). This raises interesting questions about the mechanism
415 of SMC5/6-mediated transcriptional silencing, since it can occur outside PML NBs. In this
416 regard, SUMOylation was recently shown to support the recombination-based alternative
417 lengthening of telomeres (ALT) pathway in the absence of PML NBs (54), which are
418 normally key components of the fully active pathway (47). Therefore, the SUMOylation of
419 plasmid associated proteins, and or SMC5/6, may support transcriptional repression of
420 plasmids in the absence of PML NBs, consistent with our findings using TAK-981.
421 Interestingly, the expression of LT enhances plasmid transcription in a non-additive
422 manner with the deletion of SIMC1 or SLF2, suggesting an epistatic relationship. While
423 LT is known to be a promiscuous transcriptional activator (55,56) that does not rule out a
424 co-existing role in antagonizing SMC5/6. Indeed, these findings are reminiscent of HBx
425 from HBV and Vpr of HIV-1, both of which are known promiscuous transcriptional
426 activators that also directly antagonize SMC5/6 to relieve transcriptional repression
427 (12,38,39,48,57-59). Unlike HBx and Vpr, the interaction of LT with SMC5/6 does not

428 appear to induce the degradation of its subunits (33). Nevertheless, LT binds and
429 sterically inhibits several cellular proteins instead of inducing their degradation, including
430 Rb and p53 (60). Further analysis will be needed to define LT-SMC5/6 contacts, and its
431 potential mode of inhibition. This will have important ramifications for the lifecycle of the
432 pathogenic polyomaviruses since their LT proteins share functions with SV40 LT (61).

433 In conclusion, our structure-function analyses delineate a specific function for the
434 SIMC1-SLF2 complex in SMC5/6-mediated plasmid repression. This resolves a
435 discrepancy in the field, wherein SLF2 was thought to act alone in ecDNA repression,
436 since SLF1 is not required. While further studies are needed, SIMC1-SLF2 is most likely
437 responsible for supporting SMC5/6-mediated ecDNA silencing, including that of multiple
438 pathogenic viruses. Although HBV silencing requires PML NBs, we find that plasmid
439 silencing does not. This represents a departure from current dogma, suggesting that the
440 SMC5/6-mediated repression mechanism does not always rely on PML NB-resident
441 factors. In some cases, the SUMOylation of ecDNA-associated proteins may be sufficient
442 to support SMC5/6-based repression. Finally, because the SV40 LT antigen interacts with
443 SMC5/6 and antagonizes its repression of plasmids, the orthologous polyomaviral LT
444 antigens are likely to block SMC5/6-mediated restriction of pathogenic polyomaviruses.
445

446 **Materials and Methods**

447 **Construction of recombinant plasmids**

448 Construction of plasmid DNA was described in (33). Mutations in SIMC1 (combo ctrl),
449 SLF2 (mut1, mut2) and SMC6 (SIMC1-facing, SLF2-facing, SIMC1-SLF2-groove-facing)
450 were either introduced in primers or a gBlock sequence containing desired mutations was
451 purchased (IDT). All plasmids created in this study have been verified by sequencing
452 service provided by Plasmidsaurus. Additional details of plasmid construction are
453 available upon request.

454

455 **Cell culture, transfection, stable line generation**

456 All cell lines and their derivatives were cultured in DMEM (Gibco, #11995065)
457 supplemented with 10% (v/v) fetal bovine serum (Omega Scientific, #FB-01), 1% (v/v)
458 antibiotic-antimycotic (Gibco, #15240062) and maintained at 37 °C in humidified air with
459 5% CO_2.

460 Transient plasmid transfections and generation of stable cell lines was detailed in (33). A
461 list of cell lines and vectors used for generating stable cell lines or transient transfection
462 are listed below:

cell line (*Homo-sapiens*)			
Designation	**Source or reference**	**Identifier**	**Additional information**
HEK293	DOI: 10.7554/eLife.79676		
HEK293T; U2OS	DOI: 10.7554/eLife.79676		

U2OS SIMC1$^{-/-}$	this paper	clone B9	Derived from U2OS by CRISPR/ Cas9
U2OS SLF1$^{-/-}$	this paper	clone E9	Derived from U2OS by CRISPR/ Cas9
U2OS SLF2$^{-/-}$	this paper	clone 18	Derived from U2OS by CRISPR/ Cas9
U2OS PML$^{-/-}$	DOI: 10.1101/gad.333963.119	clone 2C	
RPE	DOI: 10.1101/gad.333963.119		
Lentiviral vectors to generate stable cell line			
pHAGE2-FLAG-SIMC1	DOI: 10.7554/eLife.79676	pNB185	
pHAGE2	DOI: 10.7554/eLife.79676	pNB248	
pHAGE2-FLAG-SLF2	this paper	pNB525	
pHAGE2-FLAG-SLF2 mut1	this paper	pNB527	SLF2 mutations E1121A/ K1122A/ K1125D/ C1126R/ E1130K
pHAGE2-Flag-SLF1	this paper	pNB555	
pHAGE2-LT	this paper	pNB648	
pHAGE2-GFP	this paper	pNB670	
pHAGE2-LT-HR684	this paper	pNB717	
pMD2G	Addgene	#12259	
psPAX2	Addgene	#12260	
Vectors used for transient transfection			
pDEST-eGFP-NLS-STOP	Helle Ulrich lab	pNB68, pNZ110	

Dual secreted luciferase reporter	Addgene	#181934 pNB671	EF1alpha-Gaussia luciferase, CMV-Cypridina luciferase
pBlueScript KS-SV40	DOI: 10.1371/journal.ppat.1002949	pNB371	strain 776
pDEST-eGFP-SIMC1	DOI: 10.7554/eLife.79676	pNB263	
pDEST-FLAG-NLS-SLF2 (635-1173)	DOI: 10.7554/eLife.79676	pNB439	$SLF2^{CTD}$
pDEST-GFP-SIMC1 combo1 mut	DOI: 10.7554/eLife.79676	pNB497	SIMC1 mutations R473D/ N477A/ E480K/ E481K
pDEST-GFP-SIMC1 combo1 ctrl	this paper	pNB499	SIMC1 mutations Q842A/ H846A/ K849E/ D857R
pDEST-Myc-SMC6	DOI: 10.7554/eLife.79676	pNB530	
pDEST-FLAG-NLS-SLF2 (635-1160)	this paper	pNB535	
pDEST-FLAG-NLS-SLF2 (635-1173) mut1	this paper	pNB536	SLF2 mutations E1121A/ K1122A/ K1125D/ C1126R/ E1130K
pDEST-FLAG-NLS-SLF2 (635-1173) mut2	this paper	pNB537	SLF2 mutations T1138R/ K1141E/ D1142R/ A1145R/ G1149E
pDEST-GFP-SMC6	this paper	pNB546	
pDEST-GFP-SMC6 (groove-facing)	this paper	pNB677	SMC6 mutations L939A/ R940A/ K942A/ L943A
pDEST-GFP-SMC6 (SLF2-facing)	this paper	pNB678	SMC6 mutations R940A/ Y944A/ N947A
pDEST-GFP-SMC6 (SIMC1-facing)	this paper	pNB679	SMC6 mutations K942A/ D946A/ K957A
pDEST-2Myc-SIMC1	this paper	pNB680	
pDEST-Flag- LT wt	this paper	pNB739	

463

464 **Cell line generation by CRISPR/Cas9**

465 SIMC1, SLF1 and SLF2 knockout clones were generated via reverse transfection of
466 CRISPR/Cas9 Ribonucleoprotein. A mixture of three sgRNAs specific for each gene
467 (Synthego; 24 nM) was combined with 6 nM Cas9-NLS (Synthego) in reduced-serum
468 medium OptiMEM (Life Technologies, #31985062) and incubated for 10 min followed by
469 a 15 min incubation with TransIT-X2 (Mirus, #MIR6000). 6 x 10^4 cells were added and
470 plated into 12-well plates. After 72 hours, cells were diluted and plated to isolate single
471 cell clones that were genotyped to confirm successful editing. sgRNA sequences and
472 diagnostic primers used in this study:

Target gene	**Source**	**Identifier**	**Sequence 5'- 3´**
gene knockout kit – SIMC1	Synthego	Guides for human SIMC1 CRISPR/Cas9	CCACAGGGACAAACTCTGCC; CTGCTGAAAGTCATCTTCTA; ATTGTGGGGCTGCTTGTCAC
SIMC1 CRISPR diagnostic_F	this paper	oNB576	GGGCTTAGTATTTATGAGAGC
SIMC1 CRISPR diagnostic_R	this paper	oNB1023	TGAATCACTGCACCTGGTCT
gene knockout kit – SLF1	Synthego	Guides for human SLF1 CRISPR/Cas9	AGGAAAGTGGATACTAACCA; TTGATGAAACAACTTATGAA; CGTGAAGAACTGAAACGCAC
SLF1 CRISPR diagnostic_F	this paper	oNB1024	TCCCCAAAATGCATAGTTCAAAG
SLF1 CRISPR diagnostic_R	this paper	oNB1025	ACCATGGCTCATTTGGGCTA
gene knockout kit – SLF2	Synthego	Guides for human SLF2 CRISPR/Cas9	ATGGTATACATGAGTCACGT; CTCCAAAAAGCAGACCACAG; AACTGGAATTTAGCTCCCAG

SLF2 CRISPR diagnostic_F	this paper	oNB1190	CCCAAAAGGGTGCCACCAGA
SLF2 CRISPR diagnostic_R	this paper	oNB1191	CTCCATTTGCTCCTTTCTCAACC

473

474 **Co-immunoprecipitation and Western blotting**

475 GFP-labeled proteins were immunoprecipitated using the Nano-Trap magnetic agarose
476 (Chromotek) following the manufacturer's instructions. The protocol as well as whole cell
477 lysate preparation for SDS-PAGE and western blot are described in detail in (33).
478 Antibodies used for immunoblotting:

Antibody	Source	Identifier	Dilution
GFP-Trap magnetic agarose (Alpaca Monoclonal)	ChromoTek	gtma	IP: 25ul slurry
Myc-Trap magnetic agarose (Alpaca Monoclonal)	ChromoTek	ytma	IP: 25ul slurry
Anti-FLAG (Mouse monoclonal)	Sigma	F3165	1:5000
Anti-GFP (Mouse monoclonal)	Santa Cruz	sc-9996	1:10000
Anti-Myc (Mouse monoclonal)	Invitrogen	MA1-980	1:2000
Anti-PSTAIR (Mouse monoclonal)	Sigma	P7962	1:8000
Anti-SMC6 (Rabbit Polyclonal)	Bethyl	A300-237A	1:1000
Anti-SV40 LT (Mouse monoclonal)	Abcam	ab16879	1:5000
Goat Anti-Rabbit IgG, HRP (Goat Polyclonal)	Invitrogen	31460	1:5000
Goat Anti-mouse IgG, HRP (Goat Polyclonal)	Invitrogen	31430	1:5000

479

480 **RNA extraction and quantitative PCR**

481 For monitoring SLF2 and GFP expression by qPCR, cells were harvested for RNA
482 isolation 72 hours after GFP vector transient transfection. Total RNA precipitated using
483 RNeasy Plus Mini kit (Quiagen, #74104) was treated with DNaseI kit (Invitrogen,

484 #18068-015) before cDNA synthesis by SuperScript III First-Strand Synthesis System for
485 RT-PCR (Invitrogen, #18080-051). SensiFAST SYBR No-ROX kit (Meridian Bioscience,
486 #BIO-98020) was used for qPCR and gene expression was calculated as $2^{-\Delta Ct}$ using beta-
487 actin as a reference. Oligonucleotides used for RT-qPCR:

Target gene	**Source**	**Identifier**	**Sequence 5'- 3´**
SLF2_F	this paper	oNB390	GGAAGTCACTATTCATTC
SLF2_R	this paper	oNB476	GAATTTAGCTCCCAGTGGG
GFP_F	this paper	oNB1220	AGAAGAACGGCATCAAGG
GFP_R	this paper	oNB1221	GCTCAGGTAGTGGTTGTC
beta actin_F	DOI: 10.7554/eLife.79676	oNB492	AGGCACCAGGGCGTGAT
beta actin_R	DOI: 10.7554/eLife.79676	oNB493	GCCCACATAGGAATCCTTCTGAC

488

489 **DNA extraction for qPCR**

490 U2OS cells (1 x 10^5) with either integrated or transfected GFP vector (harvested 72 hours
491 after GFP vector transfection) were resuspended in 100 ul PBS and lysed in 200 µl
492 extraction buffer (0.1 M EDTA (pH 8.0), 0.5% (w/v) SDS, 10 mM Tris-Cl (pH 8.0))
493 supplemented with 40 µg Proteinase K, 5 µg RNAseA and incubated at 55 °C for 1 hour,
494 vortexed occasionally. Lysate was sonicated on Bioruptor Pico (Diagenode) in 10 cycles
495 of 15 s ON and 30 s OFF and cleared by centrifugation at 18,000 g 10 min. DNA was
496 purified using NucleoSpin Gel and PCR clean-up kit (Macherey-Nagel, #740609) with 5
497 volumes of NTB binding buffer based on manufacturer's instructions. Oligonucleotides
498 used for quantitative PCR:

Target gene	Source	Identifier	Sequence 5'- 3´
GFP_F	this paper	oNB1220	AGAAGAACGGCATCAAGG
GFP_R	this paper	oNB1221	GCTCAGGTAGTGGTTGTC
beta actin_F	this paper	oNB1378	AGAGCAAGAGAGGCATCC
beta actin_R	this paper	oNB1379	TTTCTCCATGTCGTCCCA

499

500 **Flow cytometry**

501 GFP fluorescence measurements were based on (37). GFP reporter vector was
502 transiently transfected into cells using TransIT-LT1 (Mirus, #MIR2300). After 72 hours,
503 cells were washed in PBS, dissociated using 0.25% trypsin and resuspended in DMEM.
504 For SUMOi experiments, cells were treated with 100 nM TAK-981 (Cayman Chemical,
505 #32741) or 0.1% DMSO (Sigma, #D8418) in control plates at the time of GFP vector
506 transfection. Median GFP intensity was measured on Cytoflex S (Beckman Coulter) using
507 the CytExpert software or on Aurora (Cytek) using SpectroFlo software. A minimum of
508 1100 GFP-positive cells were analyzed.

509

510 **DNA damage by laser microirradiation**

511 Protocol adapted from (62). U2OS cells (1.5 x 10^5) were plated in a 35 mm µ-Grid dish
512 (Ibidi) a day before microirradiation. Cells were treated with 50 uM angelicin
513 (ThermoFisher, #501933704) and 1 µg/ml Hoechst 33342 (Invitrogen, #H3570) for 30 min
514 before transferring to the stage incubator of LSM880 Airyscan confocal laser scanning
515 microscope (Zeiss). Using the bleaching mode in ZEN software, DNA damage was
516 induced by irradiation of a 5-pixel wide region with a 405 nm diode laser (15% power, 1

517 iteration, zoom 1, averaging 1, pixel dwell time 0.27 μs = speed 7). One hour after the
518 irradiation, cells were treated with extraction buffer (0.5% Triton X-100, 20 mM Hepes, 50
519 mM NaCl, 3 mM $MgCl_2$, 300 mM sucrose) for 2 min, washed twice in PBS, fixed in 4%
520 formaldehyde in PBS for 15 min and stained with anti-phospho-Histone H2A.X (Ser139)
521 and anti-SMC6 antibodies following the immunofluorescence protocol.
522
523 **Immunofluorescence and microscopy**
524 Immunofluorescence and confocal microscopy were done as described (33).
525 For optimal detection of SMC6, we pre-extracted the chromatin with extraction buffer (0.5%
526 Triton X-100, 20 mM Hepes, 50 mM NaCl, 3 mM $MgCl_2$, 300 mM sucrose) for 2 min on
527 ice. Antibodies used for immunofluorescence:

Antibody	Source	Identifier	Dilution
Anti-phospho-Histone H2A.X (Ser139) (Mouse monoclonal)	Sigma	05-636	1:500
Anti-PML (Mouse monoclonal)	Santa Cruz	sc-966	1:200
Anti-SMC6 (Rabbit Polyclonal)	Bethyl	A300-237A	1:500
Anti-SV40 LT (Mouse monoclonal)	Abcam	ab16879	1:400
Goat Anti-mouse IgG (H+L), Alexa Flour 488 (Goat Polyclonal)	Life Technologies	A11029	1:1000
Goat Anti-rabbit IgG (H+L), Alexa Fluor 488 (Goat Polyclonal)	Life Technologies	A11008	1:1000
Goat Anti-mouse IgG (H+L), Alexa Fluor 555 (Goat Polyclonal)	Life Technologies	A21422	1:1000
Goat Anti-rabbit IgG (H+L), Alexa Fluor 555 (Goat Polyclonal)	Life Technologies	A21428	1:1000

528

529 **Luciferase and MTT assays**

530 U2OS cells were seeded at 4 x 10^3 cells per well of a 96-well plate and transfected with
531 20 ng of luciferase reporter plasmid (expresses secreted Gaussian luciferase under
532 EF1alpha promoter) using TransIT-LT1 (Mirus) by reverse transfection. TAK-981 in
533 indicated concentrations or DMSO were added at the time of transfection and Luciferase
534 activities were measured 3 days later. Ten microliters of culture media were mixed with
535 50 ul Gaussia Luciferase Glow Assay buffer that contains freshly diluted coelenterazine
536 substrate (Pierce™ Gaussia Luciferase Glow Assay Kit, Thermo Fisher, #16160).
537 Luminescence was measured after ten minutes on a Tecan Infinite M200 plate reader
538 (Tecan Life Sciences). The number of viable cells were estimated using MTT assay kit
539 (Sigma, #M2128) following manufacturer's instructions.

540

541 **AlphaFold-Multimer Structural modeling**

542 AlphaFold-Multimer modeling (36) was performed using default settings on the following
543 protein sequences: SIMC1^{Nse5} (425-872), SLF2^{Nse6} (733-1173), and SMC6 (1-1091) .

544

545 **Material Availability**

546 All materials produced during this work are available upon written request, in keeping with
547 the requirements of the journal, funding agencies, and The Scripps Research Institute.

548

549

References

1. Hirano T. At the heart of the chromosome: SMC proteins in action. Nat Rev Mol Cell Biol. 2006;7(5):311-22.
2. Nasmyth K, Haering CH. The structure and function of SMC and kleisin complexes. Annu Rev Biochem. 2005;74:595-648.
3. Peng XP, Lim S, Li S, Marjavaara L, Chabes A, Zhao X. Acute Smc5/6 depletion reveals its primary role in rDNA replication by restraining recombination at fork pausing sites. PLoS Genet. 2018;14(1):e1007129. PMCID: PMC5779651
4. Potts PR, Yu H. The SMC5/6 complex maintains telomere length in ALT cancer cells through SUMOylation of telomere-binding proteins. Nat Struct Mol Biol. 2007;14(7):581-90.
5. Wehrkamp-Richter S, Hyppa RW, Prudden J, Smith GR, Boddy MN. Meiotic DNA joint molecule resolution depends on Nse5-Nse6 of the Smc5-Smc6 holocomplex. Nucleic Acids Res. 2012;40(19):9633-46. PMCID: PMC3479181
6. Aragon L. The Smc5/6 Complex: New and Old Functions of the Enigmatic Long-Distance Relative. Annu Rev Genet. 2018;52:89-107.
7. Raschle M, Smeenk G, Hansen RK, Temu T, Oka Y, Hein MY, Nagaraj N, Long DT, Walter JC, Hofmann K, Storchova Z, Cox J, Bekker-Jensen S, Mailand N, Mann M. DNA repair. Proteomics reveals dynamic assembly of repair complexes during bypass of DNA cross-links. Science. 2015;348(6234):1253671.
8. Irwan ID, Cullen BR. The SMC5/6 complex: An emerging antiviral restriction factor that can silence episomal DNA. PLoS Pathog. 2023;19(3):e1011180. PMCID: PMC9980727
9. Peng XP, Zhao X. The multi-functional Smc5/6 complex in genome protection and disease. Nat Struct Mol Biol. 2023;30(6):724-34. PMCID: PMC10372777
10. Abdul F, Diman A, Baechler B, Ramakrishnan D, Kornyeyev D, Beran RK, Fletcher SP, Strubin M. Smc5/6 silences episomal transcription by a three-step function. Nat Struct Mol Biol. 2022;29(9):922-31.
11. Liu HW, Roisne-Hamelin F, Gruber S. SMC-based immunity against extrachromosomal DNA elements. Biochem Soc Trans. 2023;51(4):1571-83. PMCID: PMC10586767
12. Diman A, Panis G, Castrogiovanni C, Prados J, Baechler B, Strubin M. Human Smc5/6 recognises transcription-generated positive DNA supercoils. Nat Commun. 2024;15(1):7805. PMCID: PMC11379904
13. Serrano D, Cordero G, Kawamura R, Sverzhinsky A, Sarker M, Roy S, Malo C, Pascal JM, Marko JF, D'Amours D. The Smc5/6 Core Complex Is a Structure-Specific DNA Binding and Compacting Machine. Mol Cell. 2020;80(6):1025-38 e5. PMCID: PMC8224240
14. Jeppsson K, Pradhan B, Sutani T, Sakata T, Umeda Igarashi M, Berta DG, Kanno T, Nakato R, Shirahige K, Kim E, Bjorkegren C. Loop-extruding Smc5/6 organizes transcription-induced positive DNA supercoils. Mol Cell. 2024;84(5):867-82 e5.
15. Gutierrez-Escribano P, Hormeno S, Madariaga-Marcos J, Sole-Soler R, O'Reilly FJ, Morris K, Aicart-Ramos C, Aramayo R, Montoya A, Kramer H, Rappsilber J, Torres-Rosell J, Moreno-Herrero F, Aragon L. Purified Smc5/6 Complex Exhibits DNA Substrate Recognition and Compaction. Mol Cell. 2020;80(6):1039-54 e6. PMCID: PMC7758880
16. Kim E, Barth R, Dekker C. Looping the Genome with SMC Complexes. Annu Rev Biochem. 2023;92:15-41.
17. Uhlmann F. SMC complexes: from DNA to chromosomes. Nat Rev Mol Cell Biol. 2016.
18. Adamus M, Lelkes E, Potesil D, Ganji SR, Kolesar P, Zabrady K, Zdrahal Z, Palecek JJ. Molecular Insights into the Architecture of the Human SMC5/6 Complex. J Mol Biol. 2020;432(13):3820-37.

597 19. Yu Y, Li S, Ser Z, Sanyal T, Choi K, Wan B, Kuang H, Sali A, Kentsis A, Patel DJ, Zhao
598 X. Integrative analysis reveals unique structural and functional features of the Smc5/6 complex.
599 Proc Natl Acad Sci U S A. 2021;118(19). PMCID: PMC8126833
600 20. Taschner M, Basquin J, Steigenberger B, Schafer IB, Soh YM, Basquin C, Lorentzen
601 E, Raschle M, Scheltema RA, Gruber S. Nse5/6 inhibits the Smc5/6 ATPase and modulates
602 DNA substrate binding. EMBO J. 2021;40(15):e107807. PMCID: PMC8327961
603 21. Li Q, Zhang J, Haluska C, Zhang X, Wang L, Liu G, Wang Z, Jin D, Cheng T, Wang H,
604 Tian Y, Wang X, Sun L, Zhao X, Chen Z, Wang L. Cryo-EM structures of Smc5/6 in multiple
605 states reveal its assembly and functional mechanisms. Nat Struct Mol Biol. 2024;31(10):1532-
606 42. PMCID: PMC11479838
607 22. Pradhan B, Kanno T, Umeda Igarashi M, Loke MS, Baaske MD, Wong JSK, Jeppsson
608 K, Bjorkegren C, Kim E. The Smc5/6 complex is a DNA loop-extruding motor. Nature.
609 2023;616(7958):843-8. PMCID: PMC10132971
610 23. Palecek JJ. SMC5/6: Multifunctional Player in Replication. Genes (Basel). 2018;10(1).
611 PMCID: PMC6356406
612 24. Ryu T, Spatola B, Delabaere L, Bowlin K, Hopp H, Kunitake R, Karpen GH, Chiolo I.
613 Heterochromatic breaks move to the nuclear periphery to continue recombinational repair. Nat
614 Cell Biol. 2015;17(11):1401-11. PMCID: PMC4628585
615 25. Palecek J, Vidot S, Feng M, Doherty AJ, Lehmann AR. The Smc5-Smc6 DNA repair
616 complex. bridging of the Smc5-Smc6 heads by the KLEISIN, Nse4, and non-Kleisin subunits. J
617 Biol Chem. 2006;281(48):36952-9.
618 26. Bustard DE, Ball LG, Cobb JA. Non-Smc element 5 (Nse5) of the Smc5/6 complex
619 interacts with SUMO pathway components. Biol Open. 2016;5(6):777-85. PMCID: PMC4920195
620 27. Oravcova M, Gadaleta MC, Nie M, Reubens MC, Limbo O, Russell P, Boddy MN. Brc1
621 Promotes the Focal Accumulation and SUMO Ligase Activity of Smc5-Smc6 during Replication
622 Stress. Mol Cell Biol. 2019;39(2). PMCID: PMC6321882
623 28. Pebernard S, Wohlschlegel J, McDonald WH, Yates JR, 3rd, Boddy MN. The Nse5-
624 Nse6 dimer mediates DNA repair roles of the Smc5-Smc6 complex. Mol Cell Biol.
625 2006;26(5):1617-30.
626 29. Wan B, Wu J, Meng X, Lei M, Zhao X. Molecular Basis for Control of Diverse Genome
627 Stability Factors by the Multi-BRCT Scaffold Rtt107. Mol Cell. 2019;75(2):238-51 e5. PMCID:
628 PMC6745058
629 30. Li S, Yu Y, Zheng J, Miller-Browne V, Ser Z, Kuang H, Patel DJ, Zhao X. Molecular
630 basis for Nse5-6 mediated regulation of Smc5/6 functions. Proc Natl Acad Sci U S A.
631 2023;120(45):e2310924120. PMCID: PMC10636319
632 31. Hallett ST, Schellenberger P, Zhou L, Beuron F, Morris E, Murray JM, Oliver AW.
633 Nse5/6 is a negative regulator of the ATPase activity of the Smc5/6 complex. Nucleic Acids
634 Res. 2021;49(8):4534-49. PMCID: PMC8096239
635 32. Etheridge TJ, Villahermosa D, Campillo-Funollet E, Herbert AD, Irmisch A, Watson AT,
636 Dang HQ, Osborne MA, Oliver AW, Carr AM, Murray JM. Live-cell single-molecule tracking
637 highlights requirements for stable Smc5/6 chromatin association in vivo. Elife. 2021;10. PMCID:
638 PMC8075580
639 33. Oravcova M, Nie M, Zilio N, Maeda S, Jami-Alahmadi Y, Lazzerini-Denchi E,
640 Wohlschlegel JA, Ulrich HD, Otomo T, Boddy MN. The Nse5/6-like SIMC1-SLF2 complex
641 localizes SMC5/6 to viral replication centers. Elife. 2022;11. PMCID: PMC9708086
642 34. Niu C, Livingston CM, Li L, Beran RK, Daffis S, Ramakrishnan D, Burdette D, Peiser L,
643 Salas E, Ramos H, Yu M, Cheng G, Strubin M, Delaney Iv WE, Fletcher SP. The Smc5/6
644 Complex Restricts HBV when Localized to ND10 without Inducing an Innate Immune Response
645 and Is Counteracted by the HBV X Protein Shortly after Infection. PLoS One.

646 2017;12(1):e0169648. PMCID: PMC5240991 does not alter our adherence to PLOS ONE
647 policies on sharing data and materials.
648 35. Ashkenazy H, Abadi S, Martz E, Chay O, Mayrose I, Pupko T, Ben-Tal N. ConSurf
649 2016: an improved methodology to estimate and visualize evolutionary conservation in
650 macromolecules. Nucleic Acids Res. 2016;44(W1):W344-50. PMCID: PMC4987940
651 36. Evans R, O'Neill M, Pritzel A, Antropova N, Senior A, Green T, Žídek A, Bates R,
652 Blackwell S, Yim J, Ronneberger O, Bodenstein S, Zielinski M, Bridgland A, Potapenko A,
653 Cowie A, Tunyasuvunakool K, Jain R, Clancy E, Kohli P, Jumper J, Hassabis D. Protein
654 complex prediction with AlphaFold-Multimer. bioRxiv. 2021:2021.10.04.463034.
655 37. Soboleski MR, Oaks J, Halford WP. Green fluorescent protein is a quantitative reporter
656 of gene expression in individual eukaryotic cells. FASEB J. 2005;19(3):440-2. PMCID:
657 PMC1242169
658 38. Decorsiere A, Mueller H, van Breugel PC, Abdul F, Gerossier L, Beran RK, Livingston
659 CM, Niu C, Fletcher SP, Hantz O, Strubin M. Hepatitis B virus X protein identifies the Smc5/6
660 complex as a host restriction factor. Nature. 2016;531(7594):386-9.
661 39. Dupont L, Bloor S, Williamson JC, Cuesta SM, Shah R, Teixeira-Silva A, Naamati A,
662 Greenwood EJD, Sarafianos SG, Matheson NJ, Lehner PJ. The SMC5/6 complex compacts
663 and silences unintegrated HIV-1 DNA and is antagonized by Vpr. Cell Host Microbe.
664 2021;29(5):792-805 e6. PMCID: PMC8118623
665 40. van Breugel PC, Robert EI, Mueller H, Decorsiere A, Zoulim F, Hantz O, Strubin M.
666 Hepatitis B virus X protein stimulates gene expression selectively from extrachromosomal DNA
667 templates. Hepatology. 2012;56(6):2116-24.
668 41. Cho T, Hoeg L, Setiaputra D, Durocher D. NFATC2IP is a mediator of SUMO-
669 dependent genome integrity. Genes Dev. 2024;38(5-6):233-52. PMCID: PMC11065178
670 42. Sun H, Hunter T. Poly-small ubiquitin-like modifier (PolySUMO)-binding proteins
671 identified through a string search. J Biol Chem. 2012;287(50):42071-83. PMCID: PMC3516753
672 43. Langston SP, Grossman S, England D, Afroze R, Bence N, Bowman D, Bump N, Chau
673 R, Chuang BC, Claiborne C, Cohen L, Connolly K, Duffey M, Durvasula N, Freeze S, Gallery M,
674 Galvin K, Gaulin J, Gershman R, Greenspan P, Grieves J, Guo J, Gulavita N, Hailu S, He X,
675 Hoar K, Hu Y, Hu Z, Ito M, Kim MS, Lane SW, Lok D, Lublinsky A, Mallender W, McIntyre C,
676 Minissale J, Mizutani H, Mizutani M, Molchinova N, Ono K, Patil A, Qian M, Riceberg J, Shindi
677 V, Sintchak MD, Song K, Soucy T, Wang Y, Xu H, Yang X, Zawadzka A, Zhang J, Pulukuri SM.
678 Discovery of TAK-981, a First-in-Class Inhibitor of SUMO-Activating Enzyme for the Treatment
679 of Cancer. J Med Chem. 2021;64(5):2501-20.
680 44. Boggio R, Colombo R, Hay RT, Draetta GF, Chiocca S. A mechanism for inhibiting the
681 SUMO pathway. Mol Cell. 2004;16(4):549-61.
682 45. Boulanger M, Chakraborty M, Tempe D, Piechaczyk M, Bossis G. SUMO and
683 Transcriptional Regulation: The Lessons of Large-Scale Proteomic, Modifomic and Genomic
684 Studies. Molecules. 2021;26(4). PMCID: PMC7915335
685 46. Yao Q, Peng B, Li C, Li X, Chen M, Zhou Z, Tang D, He J, Wu Y, Sun Y, Li W. SLF2
686 Interacts with the SMC5/6 Complex to Direct Hepatitis B Virus Episomal DNA to Promyelocytic
687 Leukemia Bodies for Transcriptional Repression. J Virol. 2023;97(7):e0032823. PMCID:
688 PMC10373549
689 47. Loe TK, Li JSZ, Zhang Y, Azeroglu B, Boddy MN, Denchi EL. Telomere length
690 heterogeneity in ALT cells is maintained by PML-dependent localization of the BTR complex to
691 telomeres. Genes Dev. 2020;34(9-10):650-62. PMCID: PMC7197349
692 48. Murphy CM, Xu Y, Li F, Nio K, Reszka-Blanco N, Li X, Wu Y, Yu Y, Xiong Y, Su L.
693 Hepatitis B Virus X Protein Promotes Degradation of SMC5/6 to Enhance HBV Replication. Cell
694 Rep. 2016;16(11):2846-54. PMCID: PMC5078993

49. Fine DA, Rozenblatt-Rosen O, Padi M, Korkhin A, James RL, Adelmant G, Yoon R, Guo L, Berrios C, Zhang Y, Calderwood MA, Velmurgan S, Cheng J, Marto JA, Hill DE, Cusick ME, Vidal M, Florens L, Washburn MP, Litovchick L, DeCaprio JA. Identification of FAM111A as an SV40 host range restriction and adenovirus helper factor. PLoS Pathog. 2012;8(10):e1002949. PMCID: PMC3475652

50. Ngo AM, Puschnik AS. Genome-Scale Analysis of Cellular Restriction Factors That Inhibit Transgene Expression from Adeno-Associated Virus Vectors. J Virol. 2023;97(4):e0194822. PMCID: PMC10134838

51. Irwan ID, Bogerd HP, Cullen BR. Epigenetic silencing by the SMC5/6 complex mediates HIV-1 latency. Nat Microbiol. 2022;7(12):2101-13. PMCID: PMC9712108

52. Hofmann S, Plank V, Groitl P, Skvorc N, Hofmann K, Luther J, Ko C, Zimmerman P, Bruss V, Stadler D, Carpentier A, Rezk S, Nassal M, Protzer U, Schreiner S. SUMO Modification of Hepatitis B Virus Core Mediates Nuclear Entry, Promyelocytic Leukemia Nuclear Body Association, and Efficient Formation of Covalently Closed Circular DNA. Microbiol Spectr. 2023;11(3):e0044623. PMCID: PMC10269885

53. Mearini G, Nielsen PE, Fackelmayer FO. Localization and dynamics of small circular DNA in live mammalian nuclei. Nucleic Acids Res. 2004;32(8):2642-51. PMCID: PMC419472

54. Zhao R, Xu M, Yu X, Wondisford AR, Lackner RM, Salsman J, Dellaire G, Chenoweth DM, O'Sullivan RJ, Zhao X, Zhang H. SUMO promotes DNA repair protein collaboration to support alternative telomere lengthening in the absence of PML. Genes Dev. 2024;38(13-14):614-30. PMCID: PMC11368244

55. Sullivan CS, Pipas JM. T antigens of simian virus 40: molecular chaperones for viral replication and tumorigenesis. Microbiol Mol Biol Rev. 2002;66(2):179-202. PMCID: PMC120785

56. Gilinger G, Alwine JC. Transcriptional activation by simian virus 40 large T antigen: requirements for simple promoter structures containing either TATA or initiator elements with variable upstream factor binding sites. J Virol. 1993;67(11):6682-8. PMCID: PMC238107

57. Qadri I, Conaway JW, Conaway RC, Schaack J, Siddiqui A. Hepatitis B virus transactivator protein, HBx, associates with the components of TFIIH and stimulates the DNA helicase activity of TFIIH. Proc Natl Acad Sci U S A. 1996;93(20):10578-83. PMCID: PMC38195

58. Aufiero B, Schneider RJ. The hepatitis B virus X-gene product trans-activates both RNA polymerase II and III promoters. EMBO J. 1990;9(2):497-504. PMCID: PMC551692

59. Felzien LK, Woffendin C, Hottiger MO, Subbramanian RA, Cohen EA, Nabel GJ. HIV transcriptional activation by the accessory protein, VPR, is mediated by the p300 co-activator. Proc Natl Acad Sci U S A. 1998;95(9):5281-6. PMCID: PMC20252

60. Ahuja D, Saenz-Robles MT, Pipas JM. SV40 large T antigen targets multiple cellular pathways to elicit cellular transformation. Oncogene. 2005;24(52):7729-45.

61. Googins MR, An P, Gauthier CH, Pipas JM. Polyomavirus large T antigens: Unraveling a complex interactome. Tumour Virus Res. 2024;19:200306. PMCID: PMC11720896

62. Tampere M, Mortusewicz O. DNA Damage Induction by Laser Microirradiation. Bio-protocol 2016;6(23):e2039.

Acknowledgements

This work was supported by NIH grants R35 GM136273 to M.N.B. and GM092740 to T.O.

Author information

Affiliations

Department of Molecular and Cellular Biology, The Scripps Research Institute, La Jolla, CA 92037, USA.

Martina Oravcová, Minghua Nie & Michael N. Boddy

San Diego Biomedical Research Institute, San Diego, CA 92121, USA.

Takanori Otomo

Contributions

Conceptualization, M.N.B., T.O. Design of Methodology, M.O., M.N., M.N.B., T.O. Writing – Original Draft, M.N.B., M.N., T.O. Writing – Review & Editing, M.O., M.N., T.O., M.N.B. Formal analysis/Investigation, M.O., M.N., M.N.B., T.O. Validation, M.O., M.N. Resources, M.O., M.N. Visualization, M.O., M.N., T.O., M.N.B. Funding acquisition, M.N.B., T.O. Supervision, M.N.B., T.O. Project administration, M.N.B.

Corresponding authors:

Correspondence to Michael N. Boddy and Takanori Otomo.

Ethics declarations

Competing interests

The authors declare no competing interests.

Supplementary figures:

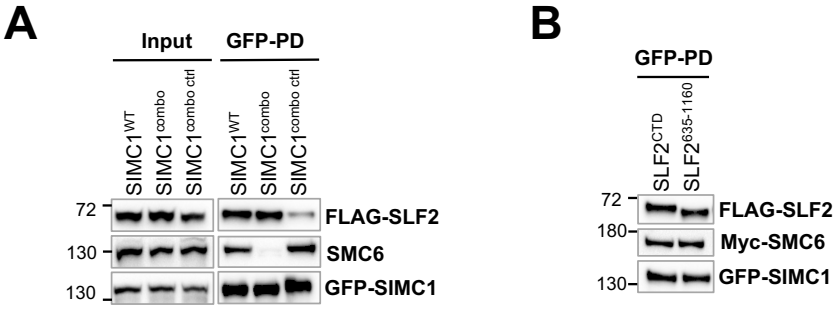

Figure 1 - figure supplement 1.
(A) Western blot of GFP-trap immunoprecipitation from HEK293 cells transiently transfected respectively with GFP-SIMC1, GFP-SIMC1 combo mutant or GFP-SIMC1 combo control mutant in combination with FLAG-SLF2^{CTD} and Myc-SMC6. Signals were detected using FLAG, SMC6 and GFP antibodies. **(B)** Western blot of GFP-trap immunoprecipitation from HEK293 cells transiently transfected with either FLAG-SLF2^{CTD} or FLAG-SLF2$^{635-1160}$ co-transfected with GFP-SIMC1 and Myc-SMC6. Signals were visualized using FLAG, Myc and GFP antibodies.

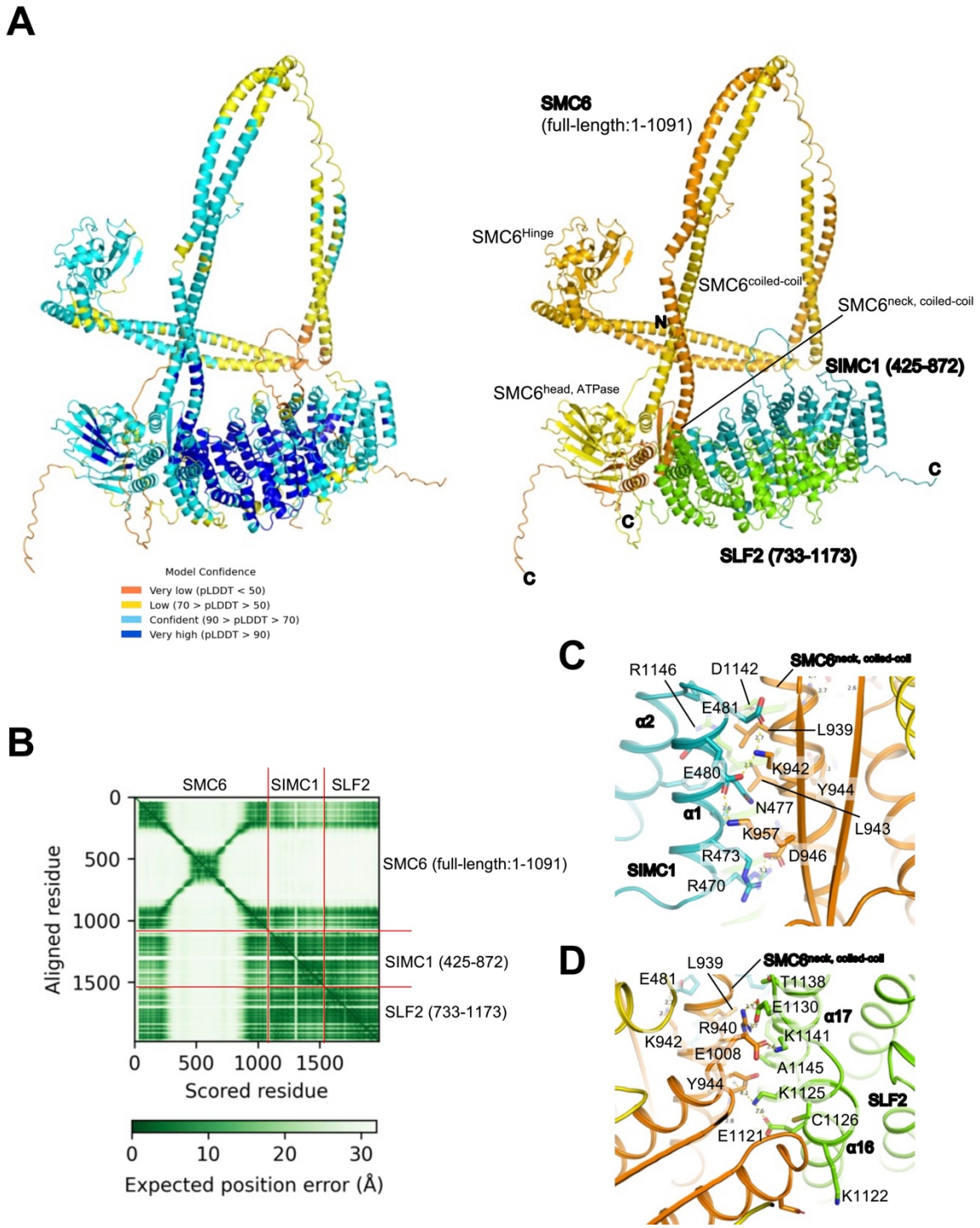

Figure 2 - figure supplement 1

(A) The AlphaFold-Multimer model of the SIMC1^{Nse5} (425-872)-SLF2^{Nse6} (733-1173)-SMC6 (1-1091) complex. The entire model is shown, colored according to pLDDT values (left) or in the same manner as in **Figure 2A**. **(B)** The Predicted Aligned Error (PAE) plot of the AlphaFold-Multimer prediction. **(C, D)** Close-up views of the SMC6 neck-SIMC1 (C) and SMC6 neck-SLF2 (D) interfaces.

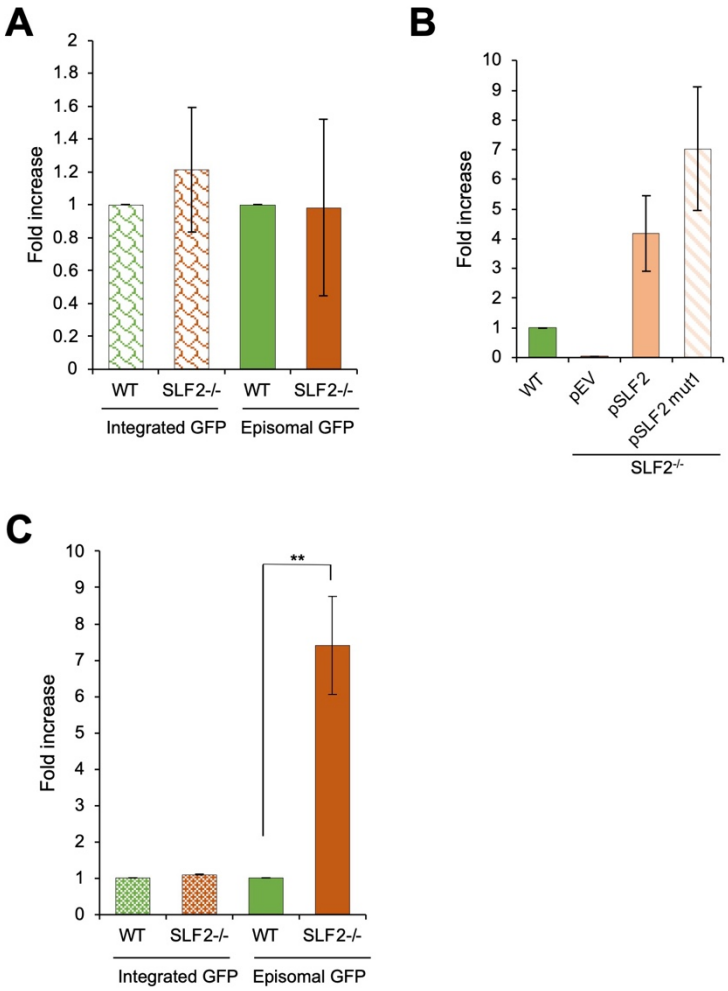

Figure 3 - figure supplement 1

(A) DNA from U2OS WT or SLF2$^{-/-}$ cells harboring either integrated or transiently transfected GFP plasmid was isolated 72 hours after transfection, GFP content was analysed by quantitative PCR and normalized to beta-actin (mean ± s.d. from n=3 independent experiments, two-tailed unpaired t-test; p>0.05). **(B)** Expression of endogenous and integrated SLF2 WT or SLF2^{mut1} in U2OS WT or SLF2$^{-/-}$ cells was measured by reverse transcription-quantitative PCR and normalized to beta-actin (mean ± s.d. from n=5 independent experiments). **(C)** GFP intensity from integrated or transfected GFP vector was measured by flow cytometry 72 hr after reporter transient transfection in U2OS WT cells or SLF2$^{-/-}$ cells. Data are the average ± s.d. from n=3 independent experiments, two-tailed unpaired t-test; (**) p-value <0.005).

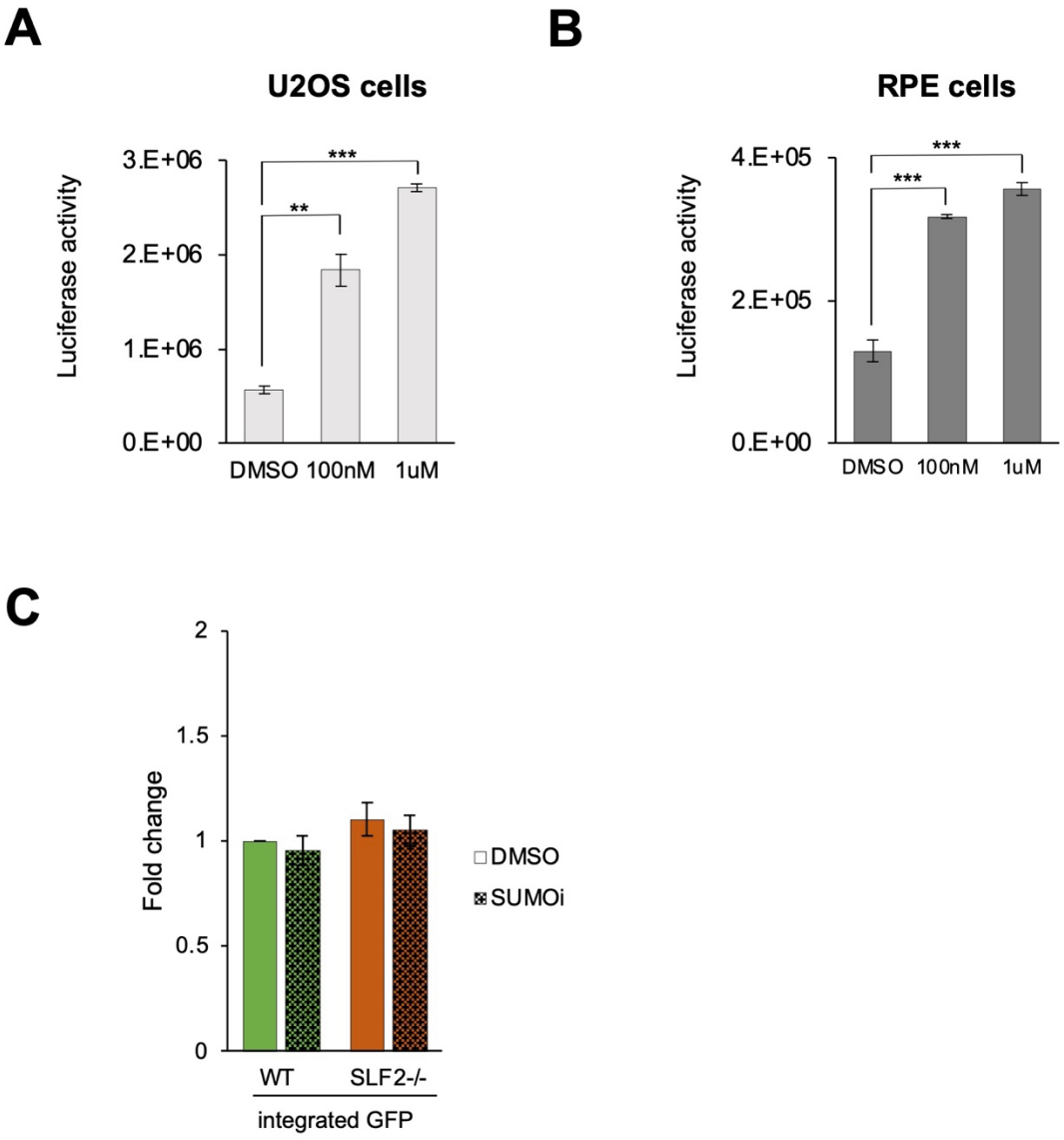

Figure 5 - figure supplement 1

Arbitrary luminescence units of U2OS (**A**) or RPE (**B**) cells expressing transfected pLuc reporter. Cells were treated with TAK-981 or DMSO at the time of transfection. Means and error bars (s.d.) were derived from a minimum of n=3 independent transfections representing biological replicates. Two-tailed unpaired t-test was performed ((∗∗) $p<0.005$; (∗∗∗) $p<0.0005$). **(C)** U2OS wt and SLF2$^{-/-}$ cells stably expressing GFP were treated with 100 nM TAK-981(SUMOi) or DMSO and GFP intensity was determined by FACS 72 hours later. Data normalized to WT cells in DMSO represent the average ± s.d. from n=3 independent experiments.

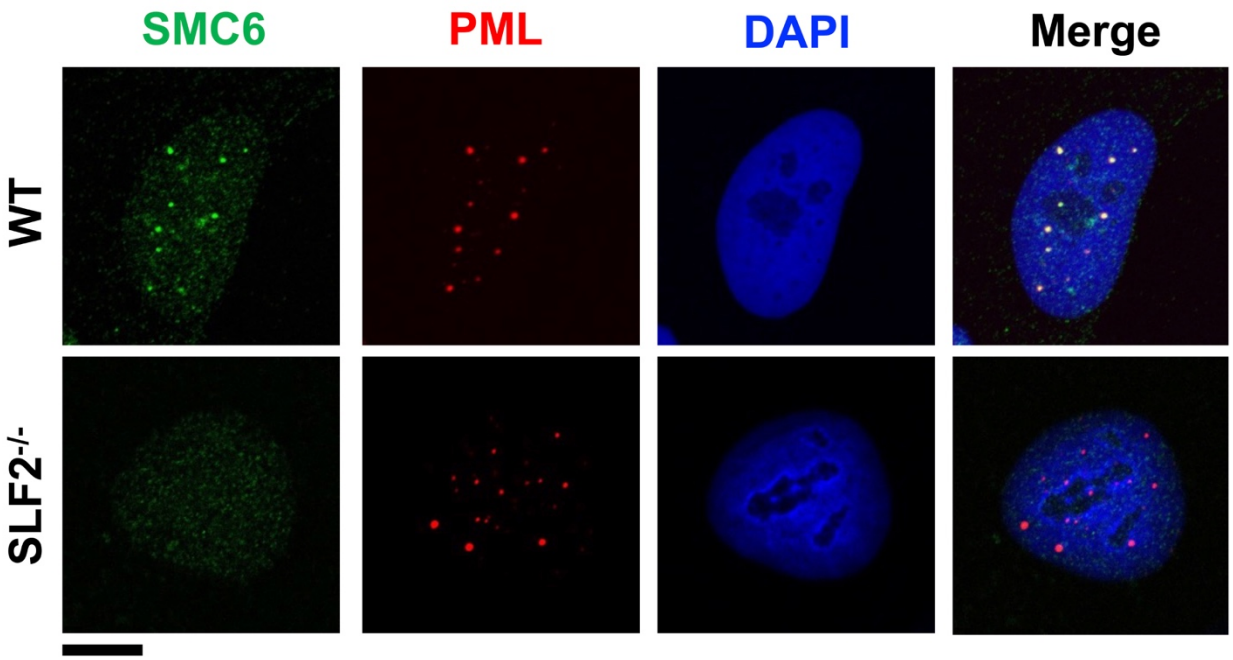

Figure 5 - figure supplement 2

Representative immunofluorescence images of U2OS WT or SLF2$^{-/-}$ cells fixed and stained with SMC6 (green) and PML (red) antibodies along with DAPI (blue). Scale bar 10 μm.

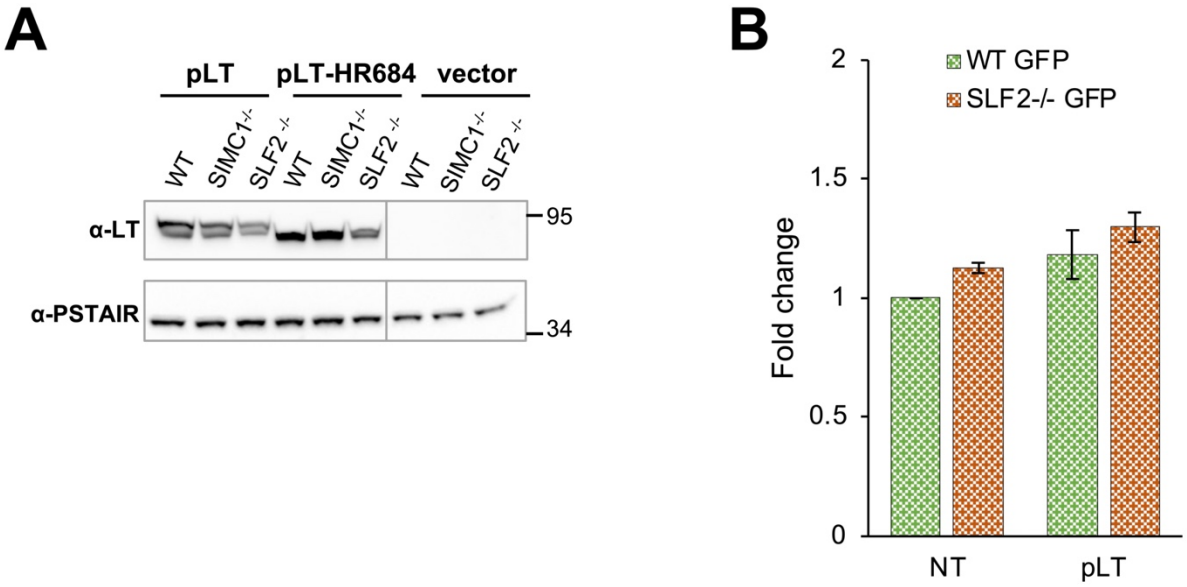

Figure 5 - figure supplement 3

(A) Immunoblot from U2OS WT, SIMC1$^{-/-}$ or SLF2$^{-/-}$ cells stably expressing large T antigen (LT), LT-HR684 variant or have an empty vector integrated, respectively. PSTAIR serves as a loading control. **(B)** U2OS wt and SLF2$^{-/-}$ cells stably expressing GFP were transiently transfected with vector expressing LT. After 72 hours, GFP intensity was measured by FACS and data normalized to non-transfected WT cells (average ± s.d. from n=3 independent experiments).

825

826 **List of Supplementary files**

827 Figure 1—figure supplement 1. A, B

828 Figure 2—figure supplement 1. A-D

829 Figure 3—figure supplement 1. A-C

830 Figure 5—figure supplement 1. A-C

831 Figure 5—figure supplement 2.

832 Figure 5—figure supplement 3. A, B

833

834 **List of source data**

835 Figure 1 – source data 1. Full and unedited blots corresponding to panel C.

836 Figure 2 – source data 1. Full and unedited blots corresponding to panel C.

837 Figure 3 – source data 1. GFP transcripts qPCR corresponding to panel A.

838 Figure 3 – source data 2. GFP FACS corresponding to panel B.

839 Figure 4 – source data 1. GFP FACS corresponding to panel B.

840 Figure 5 – source data 1. GFP FACS corresponding to panel A.

841 Figure 5 – source data 2. GFP FACS corresponding to panel B.

842 Figure 5 – source data 3. Full and unedited blots corresponding to panel C.

843 Figure 5 – source data 4. GFP FACS corresponding to panel D.

844 Figure 1 – figure supplement 1 – source data 1. Full and unedited blots corresponding

845 to panel A.

846 Figure 1 – figure supplement 1 – source data 2. Full and unedited blots corresponding

847 to panel B.

848 Figure 3 – figure supplement 1 - source data 1. GFP DNA qPCR corresponding to panel
849 A.
850 Figure 3 – figure supplement 1 – source data 2. SLF2 transcripts qPCR corresponding
851 to panel B.
852 Figure 3 – figure supplement 1 – source data 3. GFP FACS corresponding to panel C.
853 Figure 5 – figure supplement 1 - source data 1. Luciferase measurement corresponding
854 to panel A.
855 Figure 5 – figure supplement 1 - source data 2. Luciferase measurement corresponding
856 to panel B.
857 Figure 5 – figure supplement 1 - source data 3. GFP FACS corresponding to panel C.
858 Figure 5 – figure supplement 3 - source data 1. Full and unedited blots.
859 Figure 5 – figure supplement 3 - source data 2. GFP FACS corresponding to panel B.